이학박사 학위논문

A Study of Multi-modal Theranostic Particle Systems for Biological Applications

생물학적 응용이 가능한 진단·치료용 입자 시스템에 관한 연구

2016 년 2 월

서울대학교 대학원

융합과학부 나노융합전공

윤 영 일

A Study of Multi-modal Theranostic Particle Systems for Biological Applications

지도 교수 이 학 종

이 논문을 이학박사 학위논문으로 제출함

2015 년 10 월

서울대학교 대학원

융합과학부 나노융합전공

윤 영 일

윤영일의 이학박사 학위논문을 인준함

2016 년 01 월

위 원 장 김 영 훈 (인)

부위원장 이 학 종 (인)

위 원 김 연 상 (인)

위 원 박 원 철 (인)

위 원 윤 태 종 (인)

Abstract

A Study of Multi-modal Theranostic Particle Systems for Biological Applications

Young Il Yoon

Program of Nano Science and Technology

Department of Transdisciplinary Studies

Graduate School

Seoul National University

Theranostic particles, which have a dual capacity for diagnosis and therapeutics, activated by ultrasound have emerged as a novel concept for disease detection and treatment. Also, the approach could overcome intrinsic

mismatch of key metrics (e.g., pharmacokinetics, selectivity, biodistribution) between imaging and therapeutic agents, thereby allowing for precise, imaging-guided drug delivery. The technology could also open up a new opportunity for rapid assessment and adjustment of treatment regime, based on real-time imaging feedback during therapy. Many different types of theranostic agents have been developed using magnetic nanoparticles, quantum dots or novel metal nanoparticles as substrates. Existing detection modalities (e.g., magnetic resonance imaging, optical excitation) could be used to image these agents with high contrast, and often to actuate them for drug release.

Most of the developed theranostic agents, however, are still difficult to be translated into clinical applications. A significant concern is the potential toxicity of constituent materials (e.g., metal or semiconductor nanoparticles). Some agents also require specialized equipments, besides imaging instruments, to release therapeutic materials (e.g., magnetic hyperthermia, photodynamic therapy).

Microbubble (micro-meter sized bubble, MB) and liposome (Lipo) particles, conversely, are promising clinical application materials comprising non-toxic lipid chemicals. These newly developed materials can be used for the diagnosis and treatment of cancer and serve as alternatives to conventional theranostics that have known toxicological problems. Synthesized with

biocompatible polymers, these particles are shown to be non-toxic for in vivo uses. They can also be loaded with contrast agents for enhanced imaging (e.g., microscopy, MRI, ultrasound), and importantly, with therapeutic materials to treat tumor. To assess their potential in biological applications, the following chapters were studied.

The first theme herein introduces a microbubble and liposome complex (MB-Lipo) developed for ultrasound (US) imaging and activation. The MB-Lipo particles have a hybrid structure consisting of a MB complexed with multiple Lipos. The MB components are used to generate high echo signals in US imaging, while the Lipos serve as a versatile carrier of therapeutic materials. MB-Lipo allows high contrast US imaging of tumor sites. More importantly, the application of high acoustic pressure bursts MBs, which releases therapeutic Lipos and further enhances their intracellular delivery through sonoporation effect. Both imaging and drug release could thus be achieved by a single US modality, enabling in situ treatment guided by real-time imaging. The MB-Lipo system was applied to specifically deliver anticancer drug and genes to tumor cells, which showed enhanced therapeutic effect. This theme also demonstrates the clinical potential of MB-Lipo by imaging and treating tumor in vivo.

The second theme explains how the scope of the existing application is broadened. A hybrid multifunctional particle comprising of a MB, Lipo, and

an Fe ion chelated melanin nanoparticle (MNP (Fe)) was applied for ultrasound mediated cancer targeting as a theranostic agent. Also, MNP (Fe) has this hybrid multifunctional particle diagnose cancer cells.

The third theme elucidates that optimization of parameters of portable US generator can promote development in delivery of hydrophobic and hydrophilic therapeutic materials into cancer cells.

In summary, MB has an outstanding US diagnosis function of cancer and MB burst indeed improved the co-delivery of therapeutic agents and MRI contrast agent.

Keywords: Microbubble, Liposome, Melanin Nanoparticle, Ultrasound Contrast Agent, T_1-MRI Contrast Agent

Student Nunmber: 2011-30755

Contents

List of Figures

Chapter 1

Chapter 2

Chapter 3

List of Tables

Chapter 1.

Chapter 3

Chapter 1

A theranostic particle as an ultrasound imaging contrast agent and gene/drug delivery carrier

1.1. Introduction

Microbubbles (MBs) are hydrophobic gas-filled microspheres approved for diagnostic ultrasound (US) contrast imaging by the United States Food and Drug Administration (FDA). When microbubbles are exposed to US at a frequency close to their resonance frequency, they oscillate and produce sound[1-3]. In a US field with a low acoustical pressure, microbubbles exhibit stable cavitation and will oscillate around a given diameter. However, inertial cavitation occurs at higher acoustical pressures; movement of the microbubbles becomes violent, leading to destruction of the microbubbles[4].

Liposomes (Lipos) with submicrometer sizes are also composed of safe lipid structures and shows high biocompatibility and utility. A hydrophilic aqueous solution fills the liposome, allowing it to be applied as a stabilizer for chemicals, proteins, genes, or inorganic particles[5-7].

Recently, a combination of lipo and MB was proposed to have applications as a therapeutic and imaging agent[8-10]. Under higher acoustical pressure, MB destruction in the vicinity of cells can temporarily permeabilize plasma membranes in a process called sonoporation, which has been exploited as a nonviral intracellular drug and gene delivery strategy[11-14]. However, these previous systems have used anchoring on the outside of MB-Lipo complexes with cationic lipids; this may cause gradual degradation in buffer solution or

blood and has low potential for in vivo applications[15,16]. Some studies have reported efforts to insert designed drugs or siRNA molecules into liposomes to provide specific targeting[17-21].

Herein, this chapter reports a new synthetic strategy for biocompatible MB-Lipo particles with encapsulation of bioactive molecules and the comprehensive stimuli-responsive theranostics application of US. Our approach was developed to maximize the particle functionality and transferability of organic dyes, drugs, and genes under applied external sonic stimulation. The resulting MB-Lipo particle system showed dramatically enhanced drug delivery in an animal cancer model. Furthermore, external stimulation by high acoustic pressure (called flash) at a specific site could minimize the side effects of drugs or genes.

1.2. Experimental Section

1.2.1. Preparation of microbubbles (MBs)

All phospholipids compounds were purchased from Avanti Polar Lipids (Albaster, AL, USA) and used without any purification. 1,2-Dipalmitory-snglycero-3-phophatidylcholine (DPPC, 15.4 mg), dicetyl phosphate (DCP, 1.0 mg), 1,2-dipalmitorysn- glycero-3-phosphoethanolamine (DPPE, 1.2 mg), 1,2-distearoyl-sn-glycero-3-phosphoethanolamine-N-[PDP(polyethylene glycol)-2000] (DSPE-PEG-PDP, 5.0 mg), and cholesterol (3.5 mg) were dissolved in 5 mL chloroform (99.9 %, Sigma-Aldrich, St. Louis, MO, USA). To remove the solvent, the solution was evaporated for 5 min at 35 °C and freeze-dried for 24 h at -45 °C; this led to the formation of a phospholipid film. To create a lipid solution, a 2 mL mixture of glycerin, propylene, and H_2O (1:2:7, volume ratios) was added to the film and transferred to a hermetic vial (Wheaton, NJ, USA). MBs were prepared via a mechanical mixing with a high-speed shaking-device (KIMS, South Korea) and SF_6 gas filling. Fluorescein isothiocyanate (G, FITC, 1 mg, Sigma-Aldrich) was added to the lipid solution before the mixing for incorporation into the MB.

1.2.2. Preparation of liposomes (Lipos)

The Lipo particles were produced in a similar manner. DPPC (15.4 mg), DCP (1.0 mg), DPPE (1.2 mg) and cholesterol (3.5 mg) were mixed in 5 mL chloroform. A lipid film was formed after evaporation (5 min, 35 °C) and lyophilization (24 h, - 45 °C). Two milliliters of H_2O was added to the film, and the mixture was treated with sonication for 5 min at 60 °C. To make fluorescent Lipos, hydrophilic organic dye (R, Texas red, 1 mg, Sigma-Aldrich) was added to the film solution, and excess dye was removed by centrifugation (5 min, 13,000 rpm). The film solution was subjected to freezing and defrosting cycles (5 times) in liquid nitrogen and a water bath, respectively. The liposomal dispersion was extruded through a 200 nm filter using a mini-extruder at 60 °C (Avanti polar lipids, Albaster, AL). To add sulfhydryl functional group on the Lipo surface, amine-active Lipo, derived from DPPE, was treated with 5 mg 2-iminothiolane·HCl (Traut's reagent, Pierce) for 2 h at 25 °C after adjusting the pH to ~8 with 1 M $NaHCO_3$.

1.2.3. Preparation of MB-Lipo particles

0.67 mL Thiol-active MBs (13 mg/mL), derived from DSPE-PEG-PDP, were mixed with 2 mL thiolated Lipo (10 mg/mL) by shaking for 2 h at room temperature. The reaction was monitored to pyridine-2-thione releasing by

UV-Vis spectra. The 30 mg MB-Lipo particles in aqueous solution (2 mL), containing an amine functional group, were reacted with sulfosuccinimidyl-4-(N-maleimidomethyl) cyclo hexane-1-carboxylate (sulfo-SMCC, 5 mg, Sigma-Aldrich) for 3 h at 25 °C after adjusting the pH ~ 8.2 with 1 M $NaHCO_3$, to activate maleimide functional group. This particle solution was then linked to appropriate antibodies using a general conjugation procedure.

1.2.4. Doxorubicin (Dox), plasmid DNA (pGFP), and siRNA loading into MB-Lipo particles

Doxorubicin (Sigma-Aldrich) was incorporated into Lipos by the thin-film hydration and remote-loading method with an ammonium sulfate gradient. Lipid film (21.1 mg) was hydrated with 2 mL ammonium sulfate solution (250 mM), and the liposomal suspension was sequentially extruded 5 times through filters with pore sizes of 200 nm. The ammonium sulfate was removed by centrifugation (5 min, 13,000 rpm). At this point, ammonium sulfate ions were located only inside of Lipos. The liposomal dispersion and 440 μM Dox (1:1, v/v) were mixed and incubated for 2 h at 60 °C. The mixture was washed to remove unloaded Dox, and the loading capacity of Dox in Lipos was determined by measuring the concentration of Dox in the supernatant by UV-Vis spectroscopy. $Lipo_{Dox}$ particles were then complexes

with MBs as described above. To package plasmid GFP (pGFP) gene into Lipo, Lipo (21 mg) was lyophilized, and then homogenized with pGFP (10 kbp, 34 nM) and protamine (PA, 7.5 kD, 18.8 μM) solution at ratio which was optimized by electrophoresis experiments, and was added to the Lipo powder (21 mg) and shaken for 5 min at 25 °C. The gene complex containing Lipo was washed 2 times through centrifugation (5 min, 13,000 rpm) to remove unloaded gene complex, and the loading capacity was measured by UV-Vis spectroscopy. Dox and therapeutic siRNA (siSTAT3, Thermo scientific) were incorporated into Lipos simultaneously using the same procedures described above for Dox and pGFP. All functional 20 mg Lipos (2 mL in PBS) were stored at 4 °C until further complexation with 0.67 mL of MBs (13 mg/mL) and conjugation with antibodies. The anchored antibodies were quantitative analyzed by general protein assay methods[22].

1.2.5. Phantom study for echogenicity of MB-Lipo particle system

The echogenicity of MB-Lipo (15 mg/mL) was evaluated using a phantom sample. The phantom was made using plastic connecting tube with inner diameter of 2 mm, locating in the chamber filled with water. Ultrasound scanner (iU22, Philips, Bothell, WA, USA) equipped with 5-12 MHz broadband linear probe was used for imaging.

1.2.6. Transfection of pGFP into cells using MB-Lipo particle system

The day before transfection, 3×10^4 cells were seeded in the wells of a 48-well plate (BD Falcon) or confocal 4-well plate (Lab-tex, NY, USA). HER2-MB-Lipo$_{pGFP}$ (DPPC : 2.1 mM, pGFP : 0.68 nM) was added to cells in culture media containing 10 % fetal bovine serum (FBS). Following 1 h incubation, HER2-MB-Lipo$_{pGFP}$ were washed away with PBS solution. For flash application, a clinical ultrasound scanner (iU22, Philips, Bothell, WA, USA) with a 5-12 MHz broadband linear probe was used. The probe was placed in topside of the well plate, and flash pulses (MI : 0.61) were applied for 1 min. The cells were washed twice with culture media and cultured for 2 days.

1.2.7. Cell cytotoxicity assay

A 3-(4,5-dimethylthiazol-2-yl)-2,5-diphenyltetrazolium (MTT) assay kit (Invitrogen) was used to evaluate cell viability in the presence of MB-Lipo particles. SkBr3 breast cancer cells (ATCC, VA, USA) were cultured in RPMI supplemented with FBS (10 %) and penicillin and streptomycin

(1 %). Cells were maintained at 37 °C in a humidified atmosphere containing 5 % CO_2. At confluence, the cells were washed, trypsinized, and re-suspended in culture media. Cells were then seeded at a concentration of 5,000 cells/well in a 96-well tissue culture plate and allowed to grow overnight at 37 °C under 5 % CO_2. Various MB-Lipo particle solutions were added at different concentrations into the culture media, and the cells were allowed to grow for another 24 h. To test for cell viability, culture media were replaced with MTT solution. After 3 h of incubation at 37 °C under 5 % CO_2, MTT solubilization solution was added to dissolve the resulting formazan crystals. Readings were measured spectrophotometrically at a wavelength of 570 nm, with background absorbance at 690 nm, to determine cell viability.

1.2.8. Tumor rabbit model

This study was approved by the Animal Care Committee of Seoul National University Hospital (IACUC No. 12-0315) and was performed in accordance with local ethical guidelines. A total of 9 adult New Zealand white rabbits (Biogenomics, South Korea), weighing 2.5-3.0 kg each, were used in this experiment. Rabbits were anesthetized with an intramuscular injection of ketamine hydrochloride (25 mg/kg; Ketalar, Yuhan Yanghang,

South Korea) and 2 % xylazine hydrochloride (10 mg/kg; Rompun, Bayer Korea). The abdomen of the rabbit was shaved and prepared with povidone iodine. Laparotomy was performed with a 2 cm left paramedian incision to expose the left kidney. An 18-gauge needle consisting of a cannula and a core was used for tumor implantation, and one VX2 tumor fragment was placed into the lumen of the cannula. The puncture needle was directly inserted into the sub-capsular parenchyma of the left kidney, and the tumor fragment in the lumen of the needle was pushed out the core[23]. After light pressure on the implantation point to prevent bleeding and leakage of tumor tissues, the left kidney was returned to the abdominal cavity, and the abdomen wall was closed in double layers. All the procedures were performed aseptically, and tumors were allowed to grow for 2-3 weeks to reach a size of 15-30 mm in diameter.

1.2.9. Treatment with therapeutic MB-Lipo particle to the in vivo rabbit model

Trans-catheter intra-arterial administration of 1 mL HER2-MB-$Lipo_{Dox+siSTAT3}$ (15 mg/mL) was performed under fluoroscopic guidance by a interventional radiologist who had > 10 years of experience in the procedure. The same anesthesia protocol as with VX2 tumor implantation was used.

An 18-gauge catheter (BD Angiocath Plus with intravenous catheter, Becton Dickinson South Korea) was inserted into the right central auricular artery for arterial access, and a 2.0-Fr micro-catheter (Progreat, Terumo, Japan) was advanced along the 18-gauge catheter to the descending aorta by way of the external carotid artery. The central auricular artery is the major artery supplying blood to the rabbit ear. It lies in the central region of each ear and runs along the rostral edge of the ear[24]. As the central auricular branch lies beneath a thin skin sheet, it can be used to detect the left renal artery. Thus, angiography was performed to identify the renal arterial anatomy and the branching arteries feeding the tumor. When the catheter was advanced to an adequate position in the left renal artery, the prepared MB solution was infused through the catheter at rate of 6.6 mL/min (1.5 min) using an infusion pump (Genie Plus, Kent Scientific Corporation, Torrington, CT, USA) to avoid retrograde reflux of the injected materials out of the renal artery. After completing the intra-arterial injection, the microcatheter was removed from the auricular artery, and the puncture site was compressed manually for 90 s.

1.2.10. Ultrasound imaging and applying of flash in vivo

Before and during delivery of HER2-MB-Lipo through catheter, a

genitourinary radiologist with > 20 years of experience in renal ultrasound imaging performed the ultrasound imaging. All ultrasound imaging was performed with an iU22 Ultrasound scanner (Philips Healthcare, Bothell, WA, USA) equipped with a 5-12 MHz broadband linear transducer. One minute after starting of HER2-MB-Lipo injection through an infusion pump, flashes with mechanical index (MI) of 0.61 were performed during 5 minutes with pulse width of 3 s.

1.2.11. Magnetic resonance (MR) imaging of tumors

The pre-procedural MR images were acquired to evaluate presence of tumor and its size. All images were acquired on a 3.0-T clinical MR scanner (MagnetomVerio; Siemens Healthcare, Erlangen, Germany) using an 8-channel knee coil (In vivo, Gainesville, FL, USA). T2-weighted coronal True FISP images were obtained covering the both kidneys with following parameters: repetition time (TR), 5.52 ms; echo time (TE), 2.76 ms; matrix, 256×256; flip angle, 66 degrees; slice thickness, 2 mm (25 slices); number of averages, 2; bandwidth of 501 Hz/pixel; and the field of view (FOV), 150×150 mm. A T2-weighted axial turbo spin echo (TSE) images were also obtained by using following parameters: TR, 5645 ms; TE, 87 ms; matrix, 512×358; flip angle, 144 degrees; slice thickness, 3 mm (35 slices); echo

train length (ETL), 14; number of averages, 2; bandwidth of 250 Hz/pixel; and the FOV, 130×130 mm. T1-weighted axial turbo spin echo (TSE) images were also obtained with TR, 628 ms; TE, 9.1 ms; matrix, 512×369; flip angle, 140 degrees; slice thickness, 3 mm (35 slices); ETL, 4; number of averages, 2; bandwidth of 376 Hz/pixel; and the FOV, 130×130 mm.

1.3. Results and Discussion

1.3.1. Preparation of functional MB-Lipo particles

Microbubble (MB) and liposome (Lipo) were prepared in separate processes. MBs were synthesized from phospholipids and cholesterol (scheme 1-1, 1-2). A phospholipid film was produced by lyophilizing a mixture of phospholipids and cholesterol. The film was redissolved in aqueous buffer under mechanical vibration and SF_6 gas bubbling, which resulted in the formation of MBs filled with hydrophobic SF_6 gas. During this process, a relative hydrophobic dye (G, fluorescein isothiocyanate/ FITC) that was incorporated into the MB shells also was added. The prepared MBs had a spherical shape with a mean diameter of ~ 1.5 μm (Fig. 1-1a, e). In a similar way, Lipos were synthesized from a phospholipid lipid film. Instead of employing gas bubbling, we used sonication to produce small vesicles filled with water. During this process, a relative hydrophilic red fluorescent dye (R, Texas Red) was loaded into the Lipo core. The mean diameter of Lipos was ~ 200 nm as measured from cryo-tansmission electron microscopy (cryo-TEM) and dynamic light scattering (DLS) (Fig. 1-1a, e). To assemble the MB-Lipo particles, Lipos were further terminated with sulfhydryl (-SH) group and mixed with thiol-active MBs (scheme 1-3). Antibodies against human

epidermal growth factor receptor 2 (HER2) were then anchored onto the MB-Lipo particles (1.6 μM HER2 antibody per 21 mM 1,2-Dipalmitoyl-sn-glycero-3-phophatidylcholine of particles). Confocal microscopy (Fig. 1-2a) and UV-Vis spectroscopy (Fig. 1-2b) confirmed the formation of MB_G-$Lipo_R$ particles, which were included green fluorescent dye (FITC) and red fluorescent dye (Texas red). After disulfide bond formation, pyridine-2-thione molecule was released from the DSPE-PEG(2000)-PDP, which can be detected by 2 peaks at 270 and 340 nm by UV-Vis spectroscopy. DLS further confirmed that the structure integrity of MB and Lipo were maintained after the linking and antibody conjugation procedures (Fig. 1-1e).

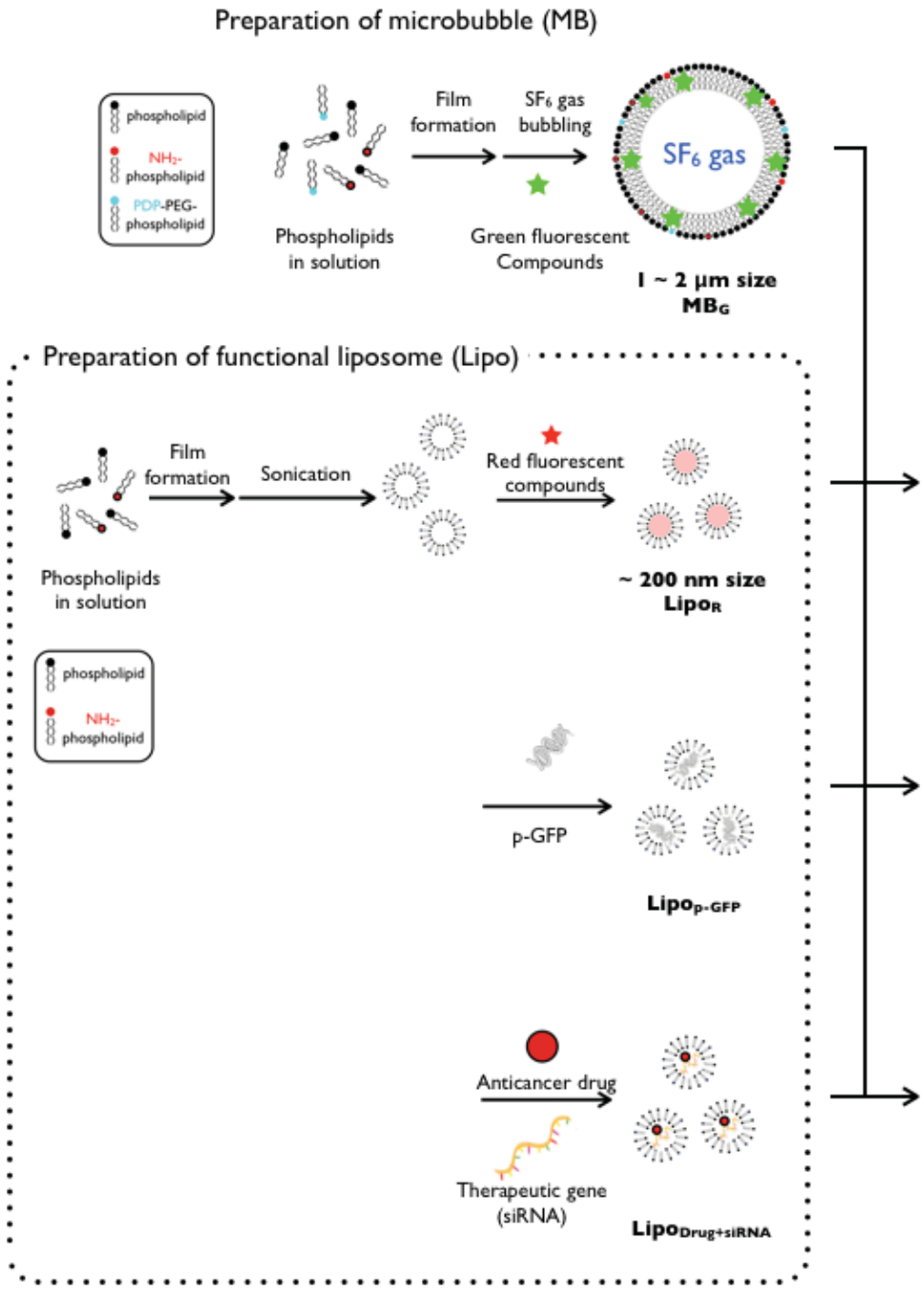

Scheme 1-1. Preparation of functional microbubble (MB), liposome (Lipo).

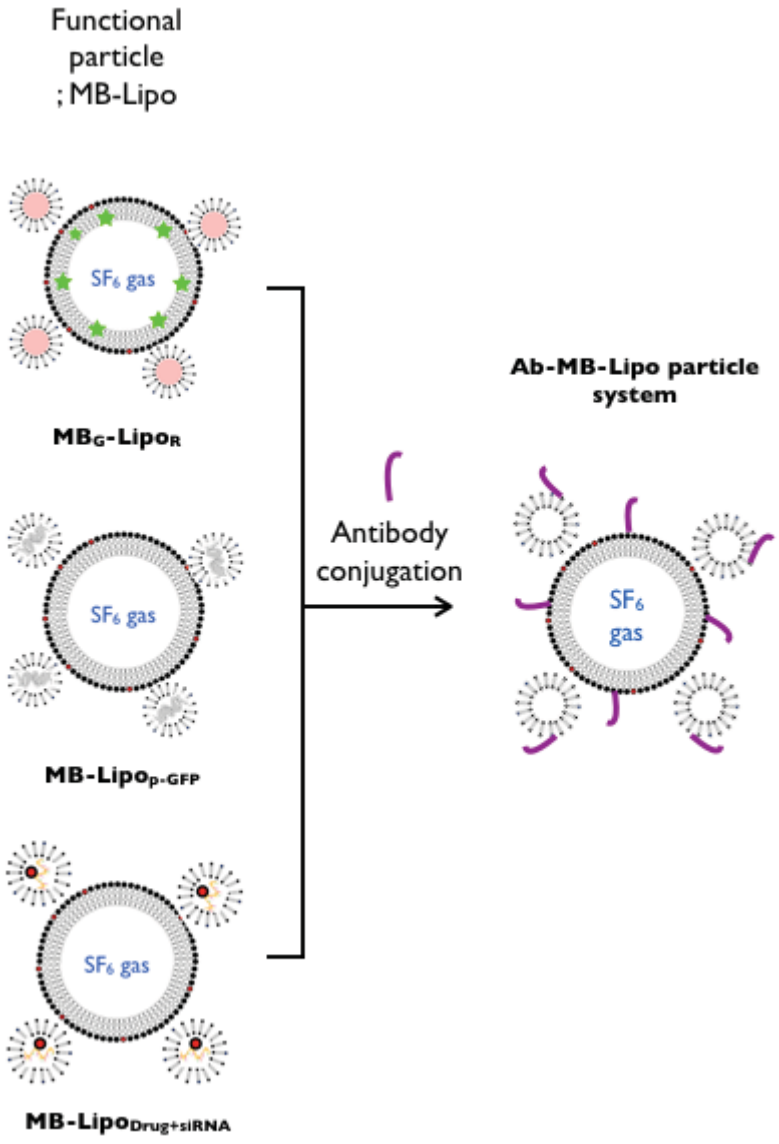

Scheme 1-2. Preparation of functional MB-Lipo and HER2-MB-Lipo.

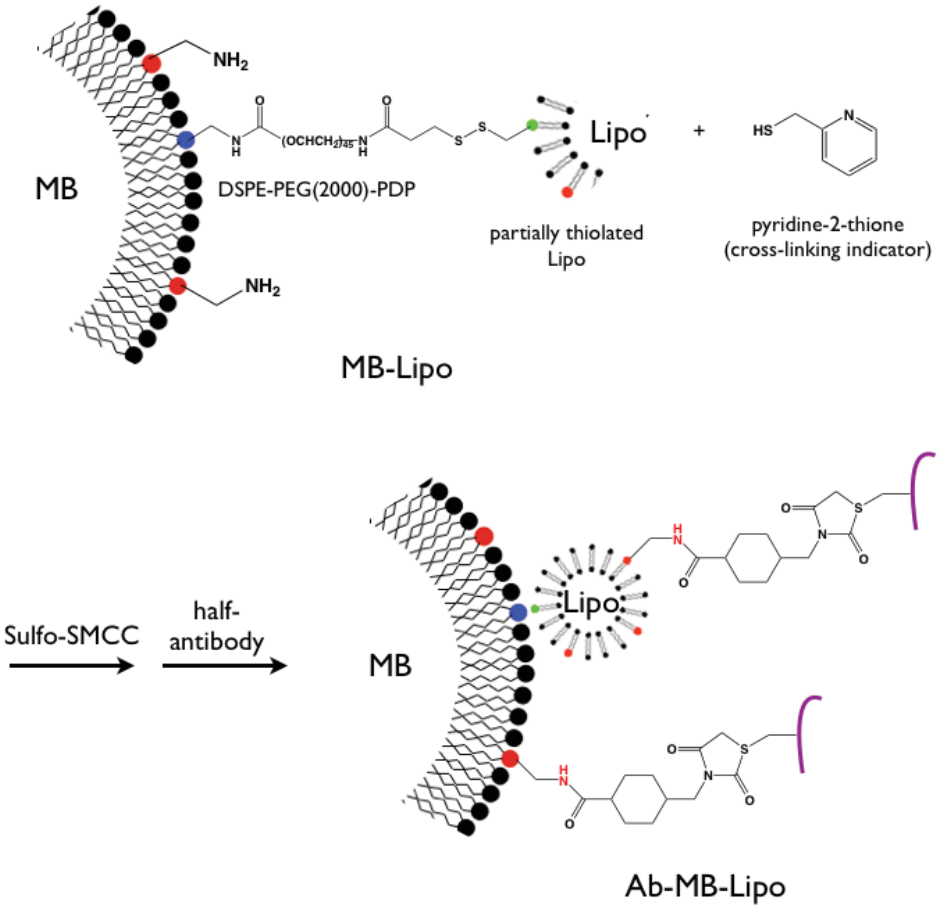

Scheme 1-3. Synthetic procedure to prepare HER2-MB-Lipo.

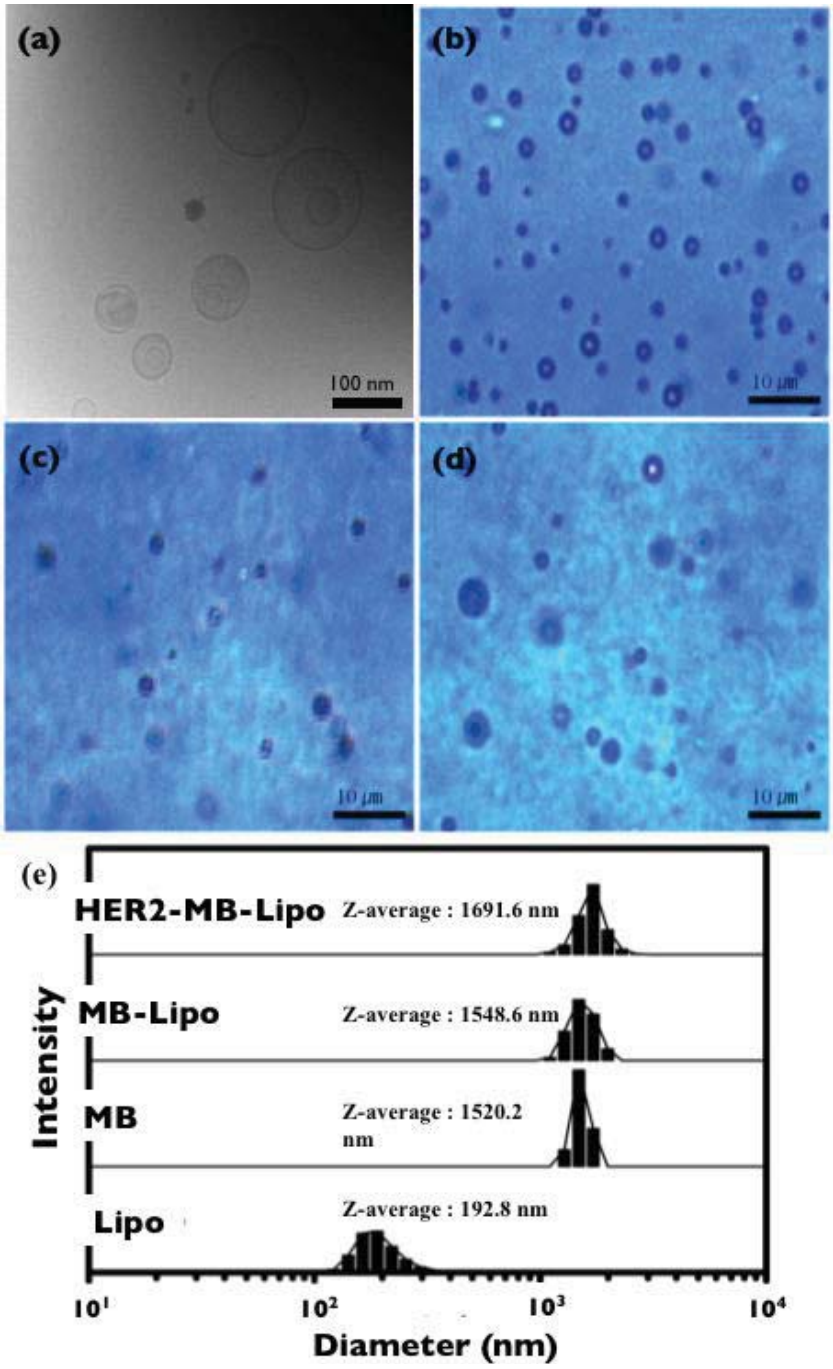

Figure 1-1. Characterization of MB-based complexes. Results of the shape and size analysis of Lipo, MB, MB-Lipo and HER2-MB-Lipo determined by cryo-TEM (a), microscopy (b-d), and DLS (e)

The HER2-MB-Lipos' echogenicity was evaluated, i.e., the capability of the particles to return US signals. Phantom samples were prepared by filling plastic tubes with HER2-MB-Lipos or commercial agents (SonoVue®, Bracco, Milan, Italy), and placed in a water bath. Samples were then imaged with a clinical US scanner (iU22, Philips, Bothell, WA, USA). The acoustic pressure, measured by the mechanical index (MI), was MI : 0.08. HER2-MB-Lipo generated a high contrast against the background (Fig. 1-3a); its performance was comparable to that of SonoVue®, which confirmed the feasibility of using HER2-MB-Lipo as US contrast agents. At elevated acoustical pressure (MI : 0.61, flash mode), MBs of HER2-MB-Lipos underwent bursting disintegration, which could be observed by a decrease of their signal intensity (Fig. 1-3b). For example, the signal from HER2-MB-Lipos gradually reduced with consecutive application of flash pulses; signal disappeared after 8 pulses. Furthermore, the HER2-MB-Lipo was stored in vials filled with SF_6 gas and demonstrated sustained signal intensity during a 2-week storage period (Fig. 1-4a), while samples in vacant vials showed decreasing intensity over time (Fig. 1-4b).

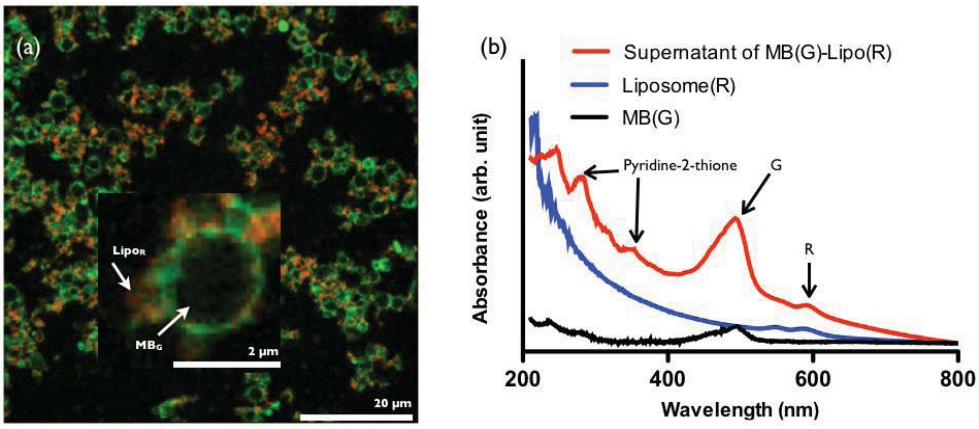

Figure 1-2. Characterization of MB-based complexes. Synthetic results of HER2-MB-Lipo analyzed by CLSM (a). Reaction results of MB with Lipo and antibody conjugation confirmed by UV-vis spectrometer (b, c)

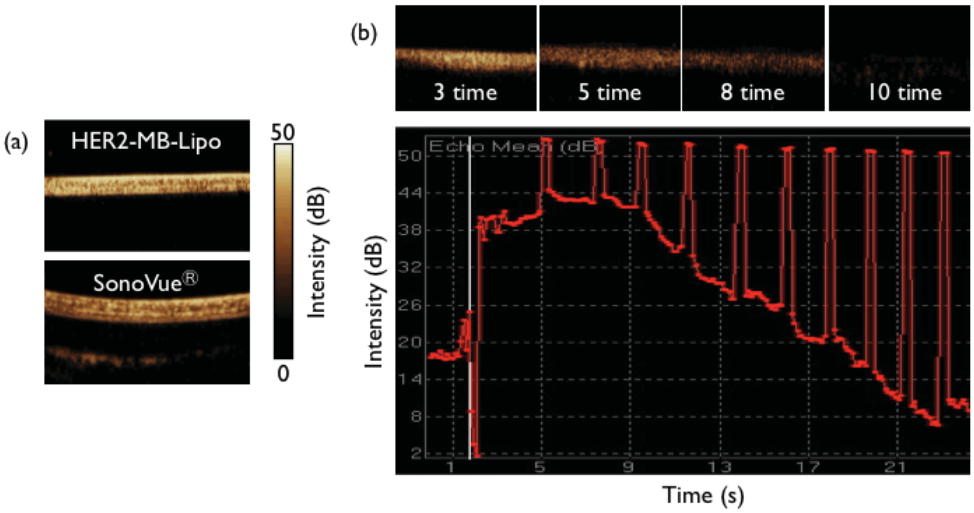

Figure 1-3. Phantom study for echogenicity of HER2-MB-Lipo (a) and destruction by flash (b).

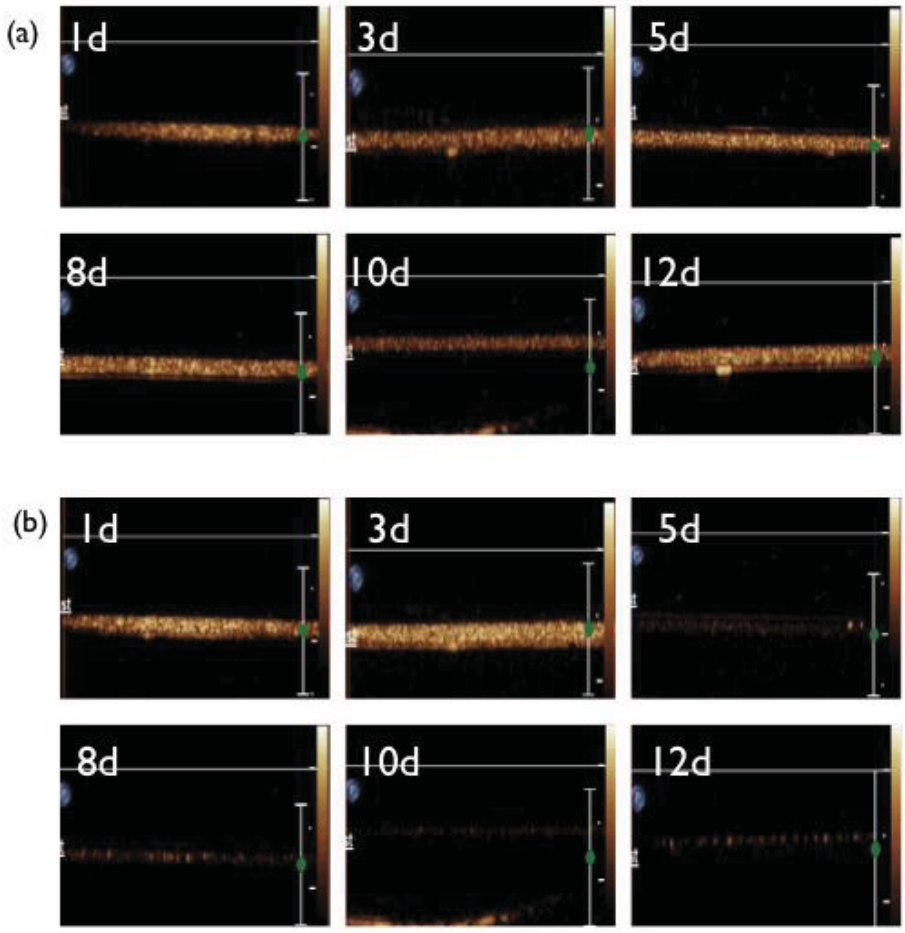

Figure 1-4. Phantom study for the stability of echogenicity in HER2-MB-Lipo.

1.3.2. Cancer cell targeting and enhanced intracellular delivery of Lipos

MB-Lipo particles could be exploited to significantly improve the delivery of Lipos into cells; burst of MBs at the flash mode not only released the attached Lipos, but also enhanced the permeability of the cell membrane (sonoporation) for more efficient Lipos uptake (scheme 1-4)[25-27]. Such effects were first investigated in vitro. Dual fluorescent MB_G-$Lipo_R$ particles (MB_G, green; $Lipo_R$, red) were prepared, and further conjugated with HER2 antibody (HER2-MB_G-$Lipo_R$). The particles were incubated with breast cancer cells (SkBr3) that over-express HER2. Confocal microscopy showed a highly selective cell targeting (Fig. 1-5). Before the application of US flash (t = 0), both green (MB) and red (Lipo) fluorescence signals were observed on the outer cell membrane, as MB-Lipo particles were not taken up by the cells presumably due to the large size of MBs (Fig. 1-5b).

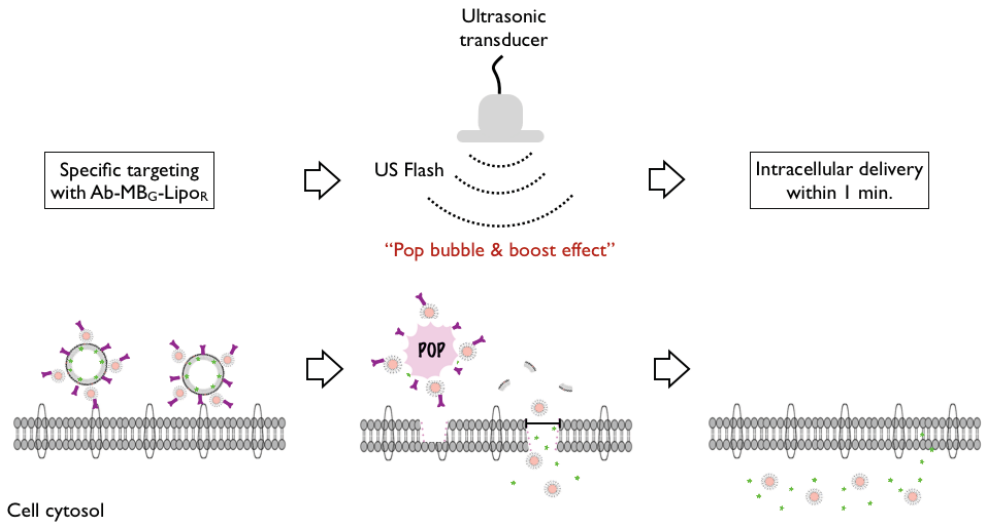

Scheme 1-4. Schematic procedure of targeting cells with HER2-MB-Lipo and inducing uptake of materials by external sonic stimulation, sonoporation, into cells.

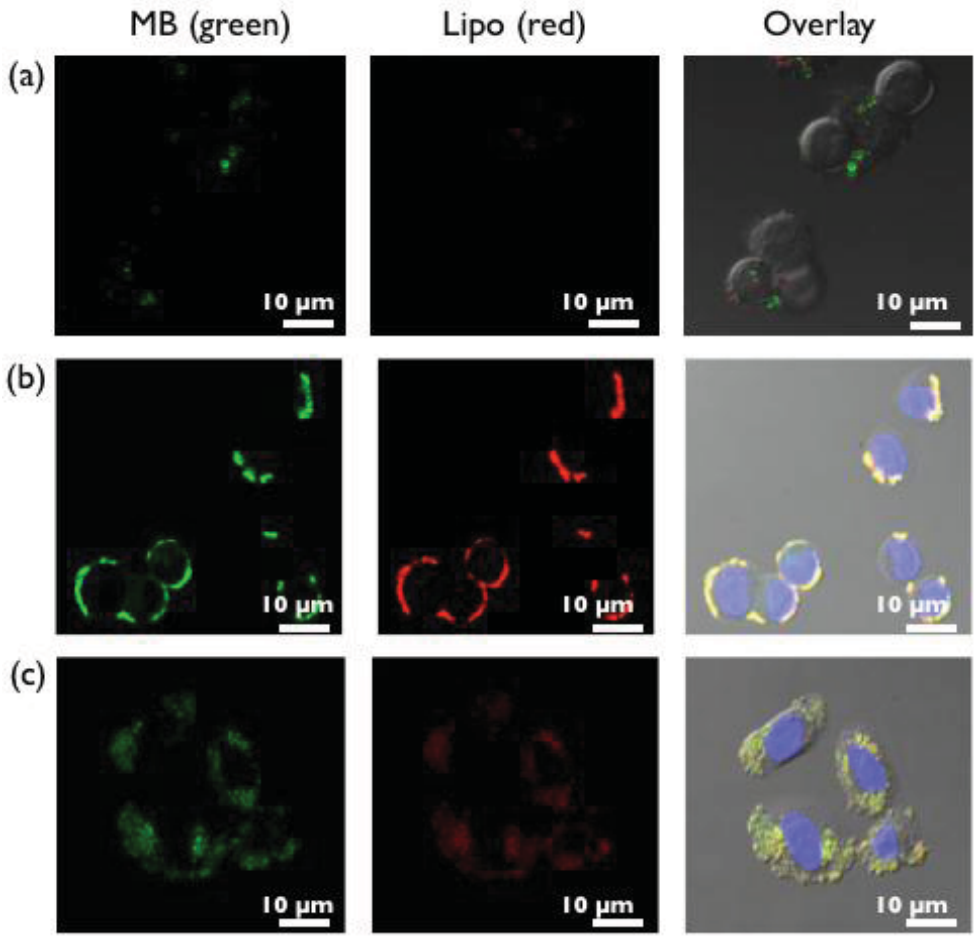

Figure 1-5. Comparison of delivery propensity by type of particle and ultrasound. CLSM results of SkBr3 cancer cell treated by MB_G-$Lipo_R$ (a), HER2-MB_G-$Lipo_R$ (b), and HER2-MB_G-$Lipo_R$ with flash (c).

The targeted cells were then exposed to US activation. I placed a 5-12 MHz linear probe into the culture dish, and applied US pulses for 1 min (MI : 0.61, flash mode). After the flash, both green and red fluorescence inside the cells were observed (Fig. 1-5c). With burst of MBs, both fluorescent dyes were released and subsequently transported into the cytoplasm. Note that MB-Lipos remained on the cellular membrane in the absence of US flash. MB_G-$Lipo_R$ particles without HER2 antibody were barely taken to nearby cells (Fig. 1-5a).

1.3.3. Application of MB-Lipo particle system as gene transfection agents

MB-Lipo particles were next utilized as a gene transfection vehicle. I reasoned that the synergistic effect of MB bursting (i.e., Lipo release and sonoporation) would significantly enhance the transport of Lipos that carry target genes. To test this hypothesis, cancer cells were transfected with plasmid green fluorescent protein (pGFP, 10 kbp) genes. To increase pGFP loading efficiency into the Lipos, the plasmid was complexed with protamine (PA, 7.5 kD)[28-30]. The optimal PA-pGFP complex ratio was 20 μM PA and 34 nM pGFP (600 PA molecules per pGFP) (Fig. 1-6a). The complex was efficiently loaded into the Lipo with ~ 95 % loading capacity which was prepared from this lipid film, and attached to MBs (Fig. 1-6b).

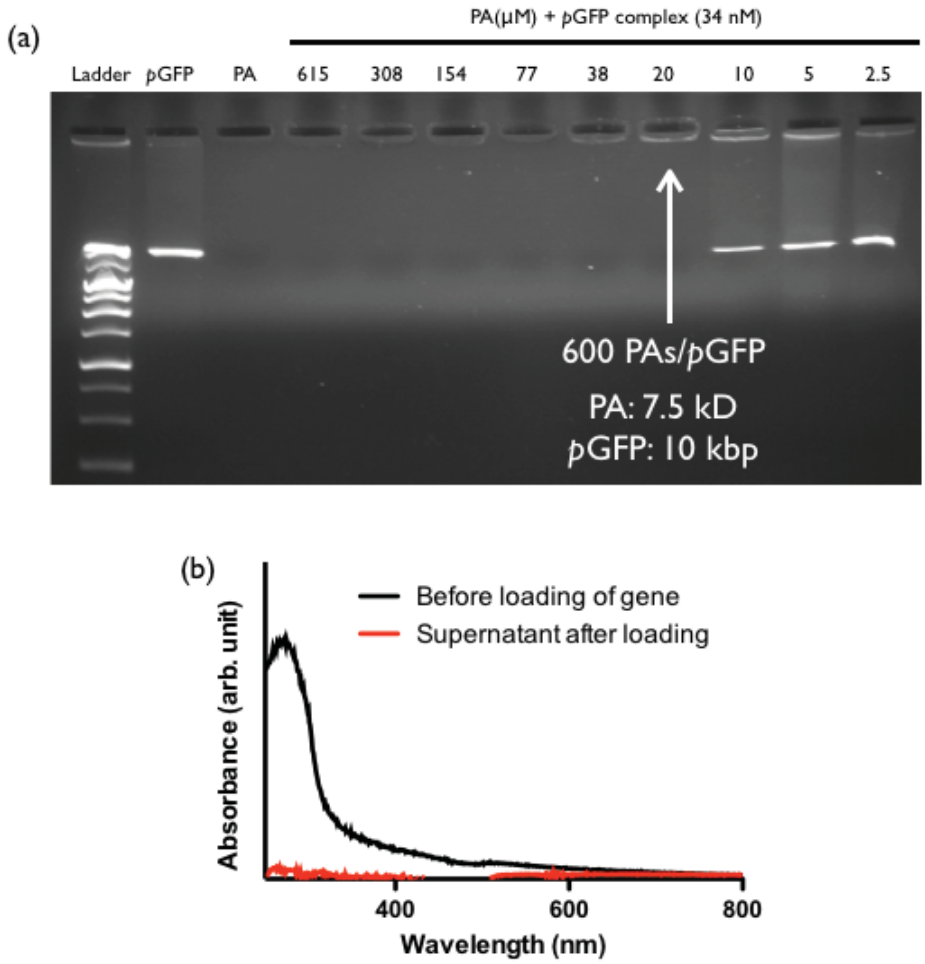

Figure 1-6. Electrophoresis results for optimizing the conjugation reaction of PA and pGFP for gene delivery study (a) and UV-vis spectrometer results of pGFP content of original before loading reaction pGFP into liposome (black line) and supernatant after loading reaction (red line) (b).

MB-Lipo$_{pGFP}$ particles were further derived with antibodies (HER2-MB-Lipo$_{pGFP}$) for cell targeting. Figure 1-7 summarizes pGFP gene transfection using the MB-Lipo particles with red fluorescent dye. Cancer cells (SkBr3) were treated with HER2-MB-Lipo$_{pGFP}$ (1 h), followed by the application of US flash (MI : 0.61) for 1 min and culture. Control samples were prepared in a similar manner, but using particles without antibody (MB-Lipo$_{pGFP}$). Microscopy analyses (48 h post flash) confirmed target-specific gene transfection; bright green fluorescence was observed in cells targeted with HER2-MB-Lipo$_{pGFP}$, while the control had negligible signal. Furthermore, MB-Lipo particle system displayed a higher transfection efficiency (~ 60 %) than a commercial agent (Lipofectamine, Invitrogen). By changing the antibody, also different cell types could be transfected with high yields. For example, cardiac fibroblasts (CFts), which are known to be difficult to transfect as a primary cell line, expressed high levels of green fluorescence when targeted with CD29-specific MB-Lipo$_{pGFP}$ and stimulated with US flash (not showed).

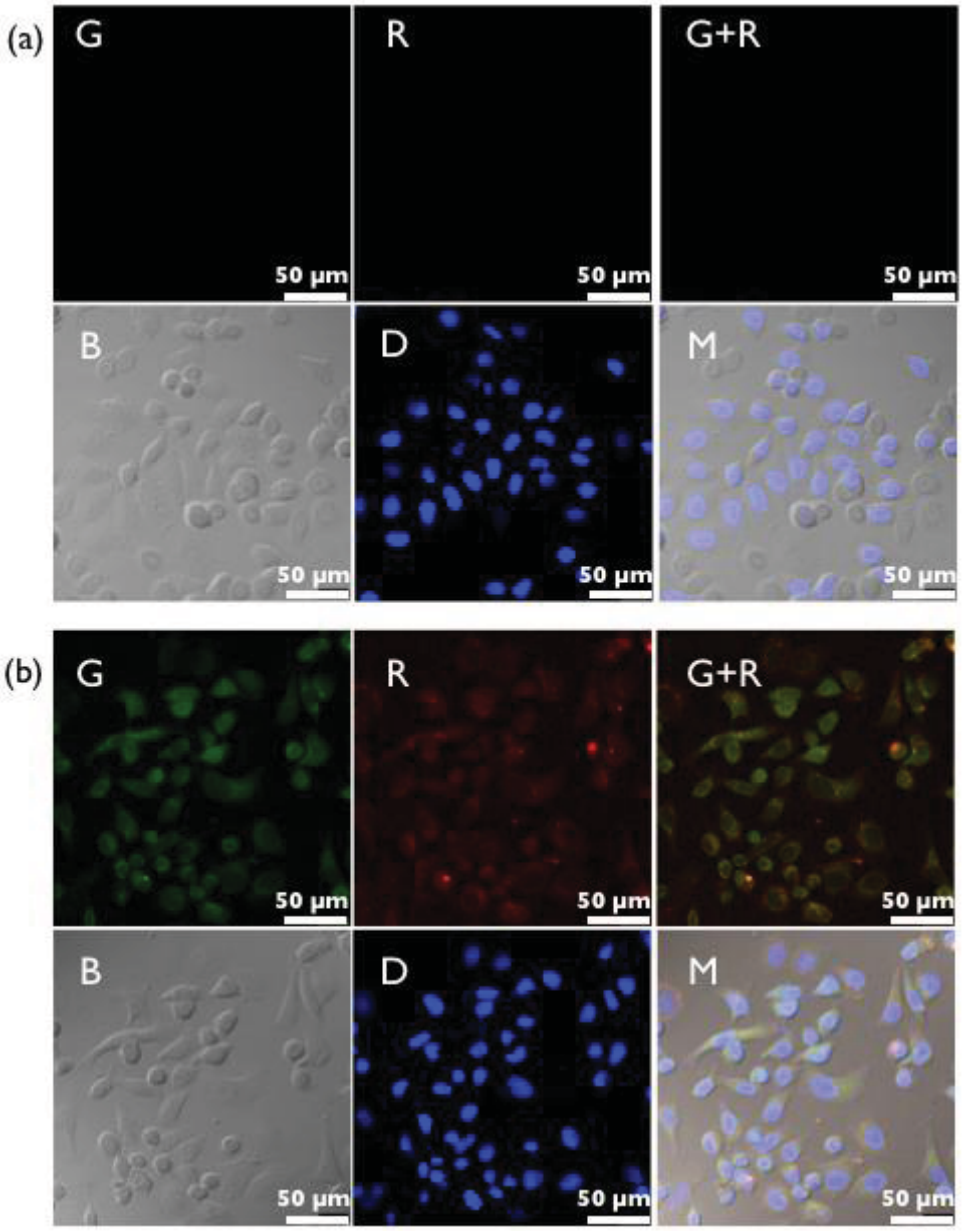

Figure 1-7. In-vitro study of particles with pGFP for gene delivery study. CLSM results of SkBr3 cancer cell non-treated (a) and treated HER2-MB-$Lipo_{pGFP}$ with flash (b). (G: green, R: red, B: bright field, D: dapi, M: merge)

1.3.4. Therapeutic application of MB-Lipo particle system as a delivery system for anticancer drugs and siRNA

The MB-Lipo particle system could serve as a versatile platform for disease treatment, as different therapeutic agents could be incorporated into liposomes. As a proof-of-concept, particles loaded with doxorubicin (Dox), an anticancer drug were prepared. Dox could be easily incorporated into the hydrophilic core of the Lipo particles using an ammonium sulfate gradient[31]. The Dox loading capacity was ~ 88.7 %, as determined by UV-Vis spectroscopy (Fig. 1-8a). Following the 1-hour incubation of cancer cells (SkBr3) with HER2-MB-Lipo$_{Dox}$ (total Dox dose, 0.19 μM), the cells were treated with US flash (MI : 0.61). The drug was efficiently penetrated into the cell nucleus (Fig. 1-8b), leading to significant cell death (35 % viability, 120 h post flash) (Fig. 1-10a, Table 1). In contrast, cells incubated with free Dox (0.19 μM, 1 h) showed 90 % viability when monitored 120 hours after the treatment. The MB-Lipo particles could also be used to deliver siRNA for therapeutic applications. As an example, Lipo was loaded with a tumor suppressor siRNA for STAT3 (signal transducer and activator of transcription 3), a transcription factor involved in cell proliferation[32, 33]. As in the case with plasmid DNA, the siRNA for STAT3 (siSTAT3) was inserted into the Lipos after PA complexation (loading capacity, 95 %). Target cells (SkBr3) were incubated

with HER2-MB-Lipo$_{STAT3}$, followed by US flashing. With the delivery of siSTAT3 to SkBr3 cells, the STAT3 gene was indeed down-regulated.

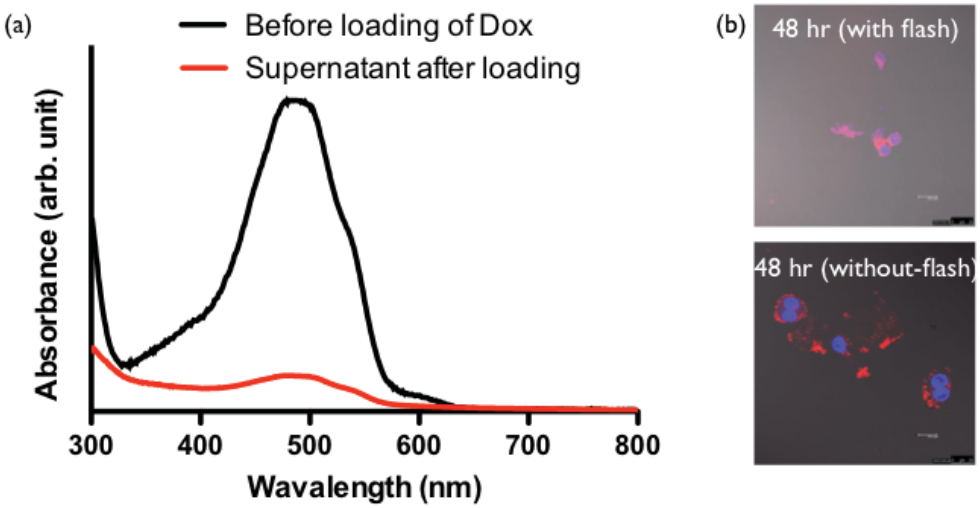

Figure 1-8. UV-vis spectrometer results of DOX content of original before loading reaction DOX into liposome (black line) and supernatant after loading reaction (red line) (a) and CLSM results of SkBr3 cancer cell treated HER2-MB-Lipo$_{DOX}$ particle without flash or with flash (b).

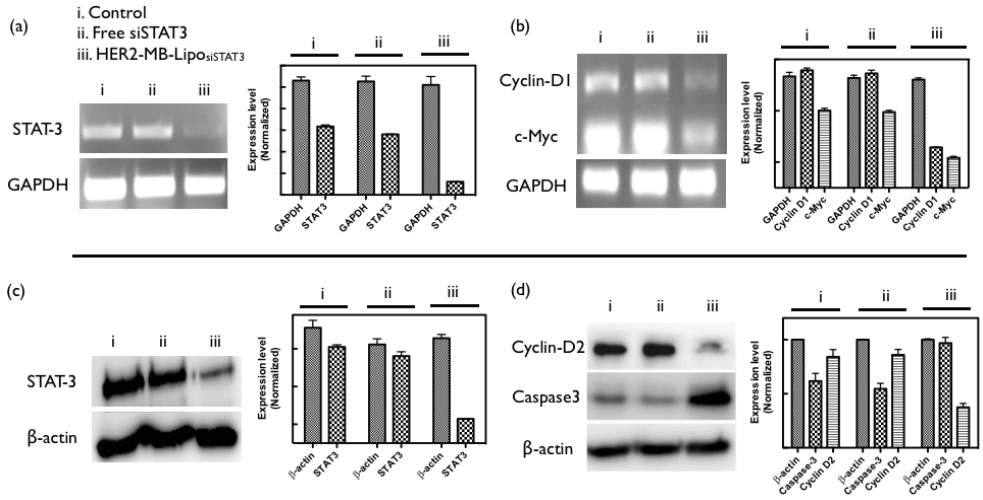

Figure 1-9. In-vitro study of particles with siSTAT3 for gene delivery study. PCR (a, b) and western blot (c, d) results of control, SkBr3 cancer cell treated by free siSTAT3, and HER2-MB-Lipo$_{siSTAT3}$ particle with flash.

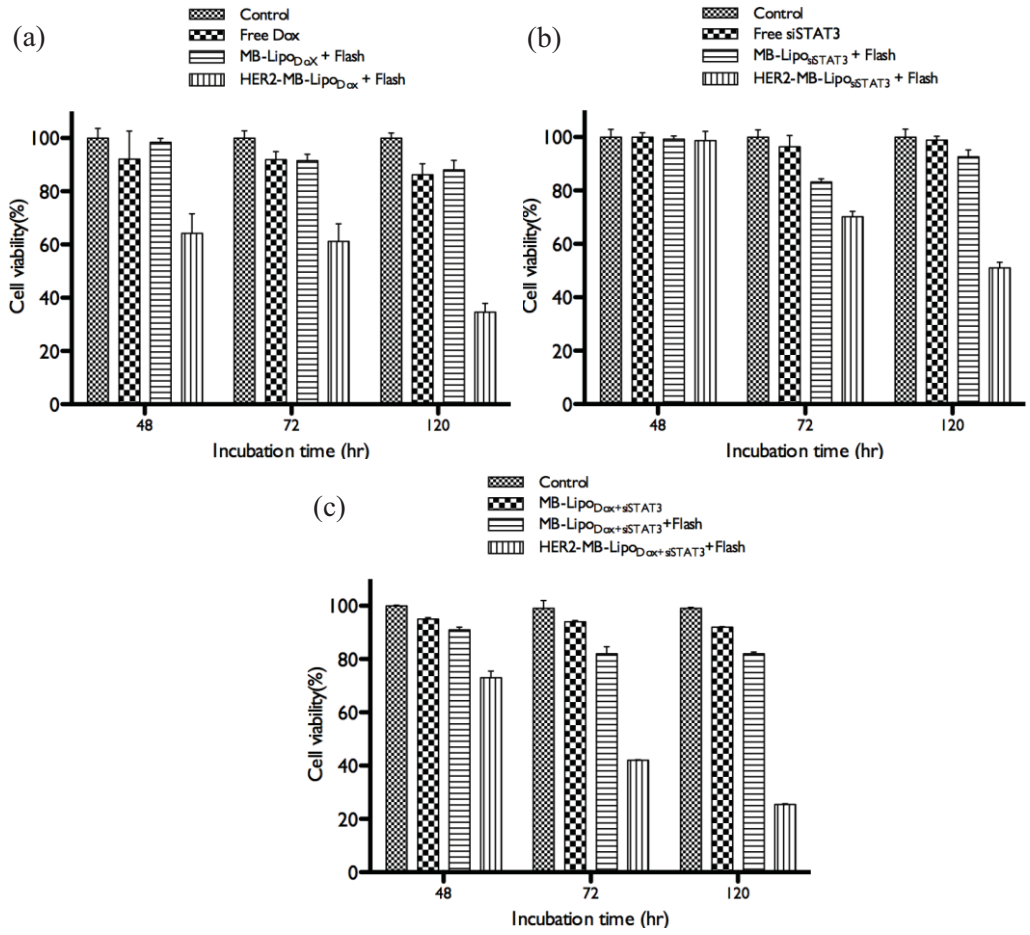

Figure 1-10. In-vitro study of various particles with DOX (a), siSTAT3 (b), and Dox + siSTAT3 (c) for drug and gene co-delivery study.

The decrease of cyclin D1 and c-Myc gene expressions was also observed, which are involved in cell proliferation (Fig. 1-9a, b)[34, 35]. Such altered gene expression changed the cellular protein expression as well (Fig. 1-9c, d). The levels of STAT-3 and cyclin D2 both decreased, whereas caspase3, an indicator of apoptosis, increased[36, 37]. The overall cell viability after the siRNA delivery was ~ 51 % (120 h post flash) (Fig. 1-10b, Table 1). Figure 1-10 summarizes the overall therapeutic efficacy of the MB-Lipo particle systems. Compared to free reagents (Dox, siSTAT3 or both), MB-Lipo agents combined with flash treatment displayed higher potency, which could be attributed to more efficient intracellular delivery of therapeutic agents. MB-Lipo particles co-delivering both Dox and siSTAT3 led to the lowest cell viability (~25 %) from synergistic effect (Fig. 10c, Table 1).

		Treatment	Cell viability (in 120 hr) Mean ± SD
Non-MB-Lipo	0.19 μM Dox or 32 nM siSTAT3	Only flash	99.9 ± 1.9
		Free Dox	86.2 ± 4.1
		Free siSTAT3	97.9 ± 3.4
MB-Lipo	Dox effect (0.19 μM Dox)	$MB\text{-}Lipo_{Dox}$ + flash	90.5 ± 4.5
		$HER2\text{-}MB\text{-}Lipo_{Dox}$ + flash	**34.6 ± 3.3**
	siSTAT3 effect (32 nM siSTAT3)	$MB\text{-}Lipo_{siSTAT3}$ + flash	92.5 ± 2.5
		$HER2\text{-}MB\text{-}Lipo_{siSTAT3}$ + flash	**51.0 ± 2.1**
	Dox + siSTAT3 effect	$MB\text{-}Lipo_{Dox+siSTAT3}$	90.4 ± 0.4
		$MB\text{-}Lipo_{Dox+siSTAT3}$ + flash	80.1 ± 1.6
		$HER2\text{-}MB\text{-}Lipo_{Dox+siSTAT3}$ + flash	**25.4 ± 0.3**

Table 1. Summary of therapeutic effect by anticancer drug (DOX) and siRNA (siSTAT3) delivery.

1.3.5. Theranostic application of MB-Lipo particle system in vivo

MB-Lipo particles were finally applied as theranostic agents in vivo. Namely, the particles were used to enhance US imaging contrast, as well as to enable US-mediated delivery of targeted gene and drug. For this demonstration, we established a rabbit renal tumor model by implanting VX2 tumor cells on the rabbit renal parenchyma. Figure 1-11a showed a photograph of implanted VX2 tumor in rabbit kidney[38]. The implanted tumor expressed HER2 as measured by immunohistochemistry (Fig. 1-11b) and Western blotting (Fig. 1-11c). HER2-specific MB-Lipo was therefore used for cell targeting, and loaded with Dox and siSTAT3 for treatment. Prepared particles (HER2-MB-$Lipo_{Dox+siSTAT3}$) were injected into the tumor sites through a catheter located in the left renal artery. Following the intra-arterial (IA) particle injection, US imaging revealed a tumor region with high contrast proffered by MBs (Fig. 1-12b). Subsequently, localized US pulses (flash, MI : 0.61, 10 times) were applied to burst MBs and deliver therapeutic-Lipos. The destruction of MBs could be monitored in situ by observing the loss of echogenicity in the targeted region (Fig. 1-12c).

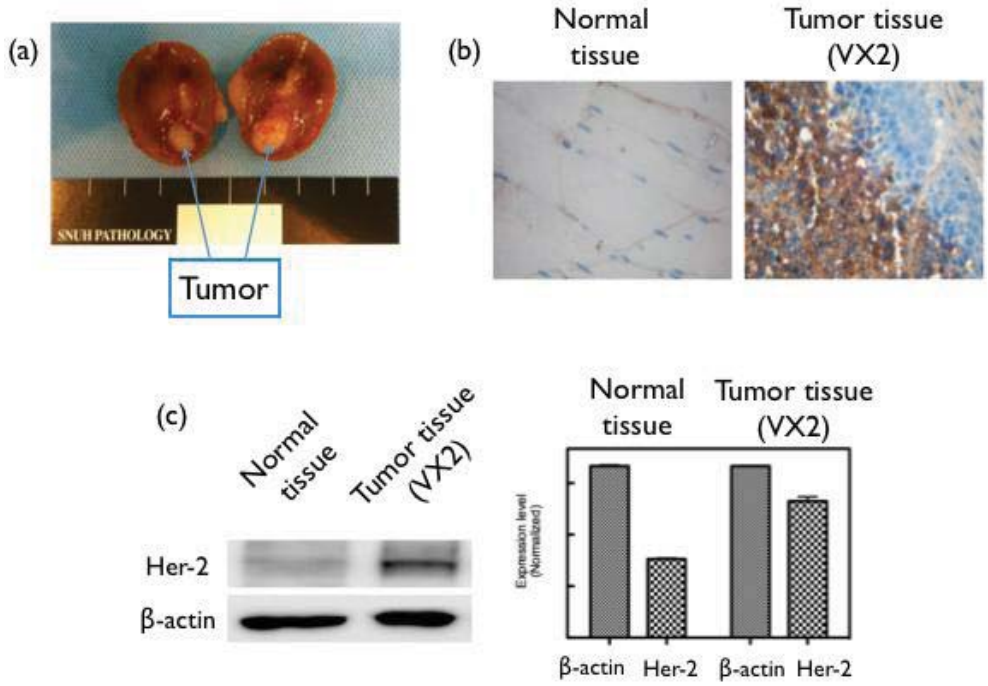

Figure 1-11. VX2 tumor in kidney of a rabbit model. Photograph of implanted VX2 tumor in rabbit kidney (a). IHC staining (b) and western blot (c) results of normal and tumor tissue (VX2).

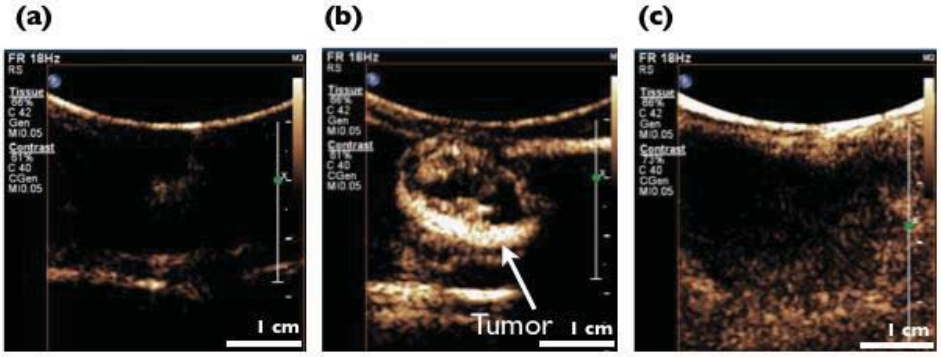

Figure 1-12. Ultrasound images of the implanted tumor (VX2) region in a rabbit kidney via IA injection. Images before IA (a), after IA (b), and after flash (c).

The accumulation of HER2-MB-Lipo$_{Dox+siSTAT3}$ into tumor sites could be attributed to the combined effect of high permeability of tumor vasculature and active targeting. In tumor microenvironment, blood vessels are shown to be defective with large gaps between endothelial cells[39, 40]. HER2-MB-Lipo$_{Dox+siSTAT3}$ thus can leak from the vessels and enter into tumor interstitium. Coating MB-Lipo$_{Dox+siSTAT3}$ with antibodies further improves the retention of MB-Lipo$_{Dox+siSTAT3}$ in tumor via receptor- mediated active targeting[41]. Local co-delivery of therapeutic agents was validated by performing microscopy and PCR analyses on the tissues extracted 4 days after US flash. The tumor tissue showed intrinsic red fluorescence of Dox (Fig. 1-14a), and the expression of the target STAT3 gene was efficiently blocked by siSTAT3 (Fig. 1-14b). Therapeutic effect was negligible in control cohorts, which was either non-targeted with particles (only flash treatment) or targeted but with no flash applied. I next sought to verify the therapeutic effect of MB-Lipo particle system on tumor growth. Figure 1-13a showed in-vivo study schedule of treating particles and imaging tumor for 10 days. HER2-MB-Lipo$_{Dox+siSTAT3}$ was administered into tumor sites on two separate days (day 1 and 5), and exposed to US flash. MR imaging was performed on days 0, 4 and 10 to analyze the tumor size and growth rate. Indeed, tumors that were treated with HER2-MB-Lipo$_{Dox+siSTAT3}$ and US flash exhibited significantly decreased growth as compared to untreated tumors and tumors not exposed to flash (Fig.

1-13b, c). Histology data on excised tumor further confirmed that the cell density of the treated tumors was lower than those of controls (Fig. 1-14c).

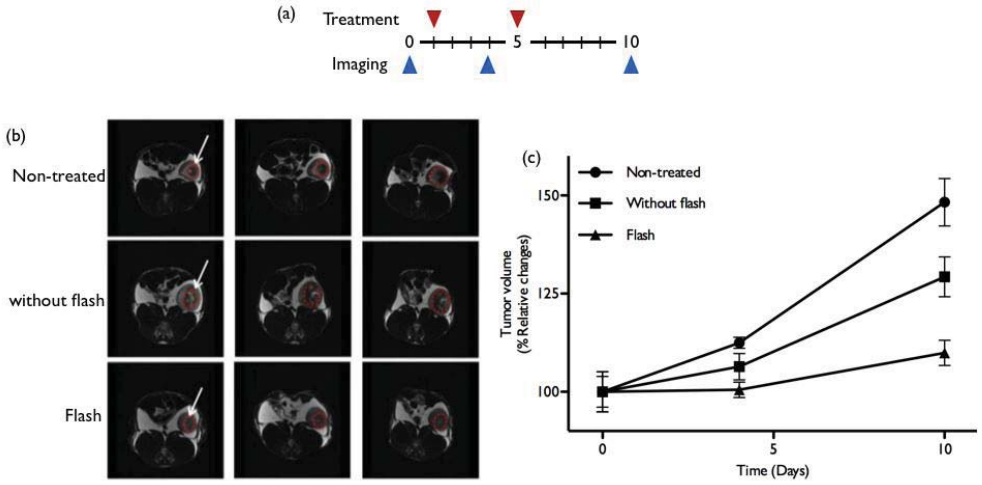

Figure 1-13. In-vivo therapeutic application of HER2-MB-Lipo$_{Dox+siSTAT3}$. In-vivo study schedule of treatment and imaging for 10 days (a). MR images (b) on day 0, 4, and 10 and tumor volume changes (c) after administrating particles. The dotted circles (red) indicate the VX2 tumor region.

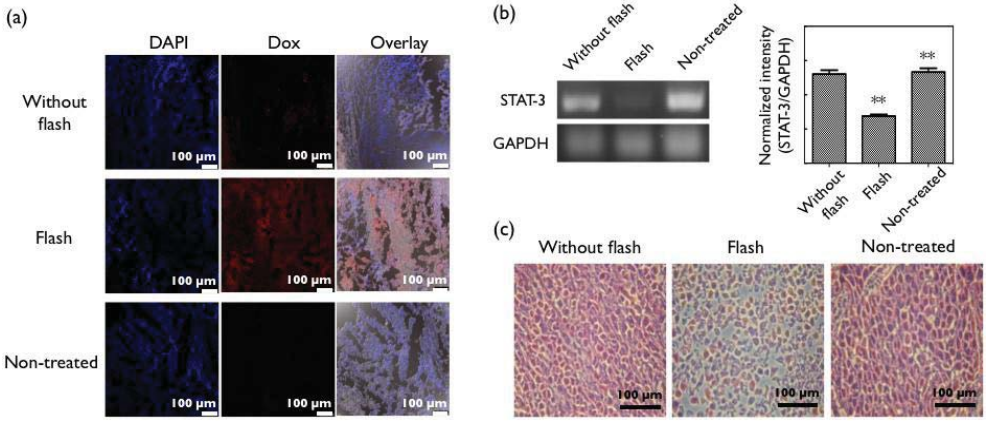

Figure 1-14. In-vivo therapeutic application of HER2-MB-Lipo$_{Dox+siSTAT3}$. CLSM (a), PCR (b), and H&E staining results (c) of extracted tumor tissue after HER2-MB-Lipo$_{Dox+siSTAT3}$ without flash or with flash.

The bio-distribution of MB-Lipo particle system after targeting and US flash was determined by analyzing the presence of fluorescent dyes in the liver, lungs, kidneys, and tumor (Fig. 1-15). For this purpose, dual fluorescent HER2-MB_G-$Lipo_R$ was used, which were intravenous injected. Majority of the particles were found in the liver and lungs, independent of exposure to flash. However, following the application of flash at the tumor site, relative high-intensity fluorescence was observed within the tumor, which showed a 3-fold increase as compared to the non-flash control.

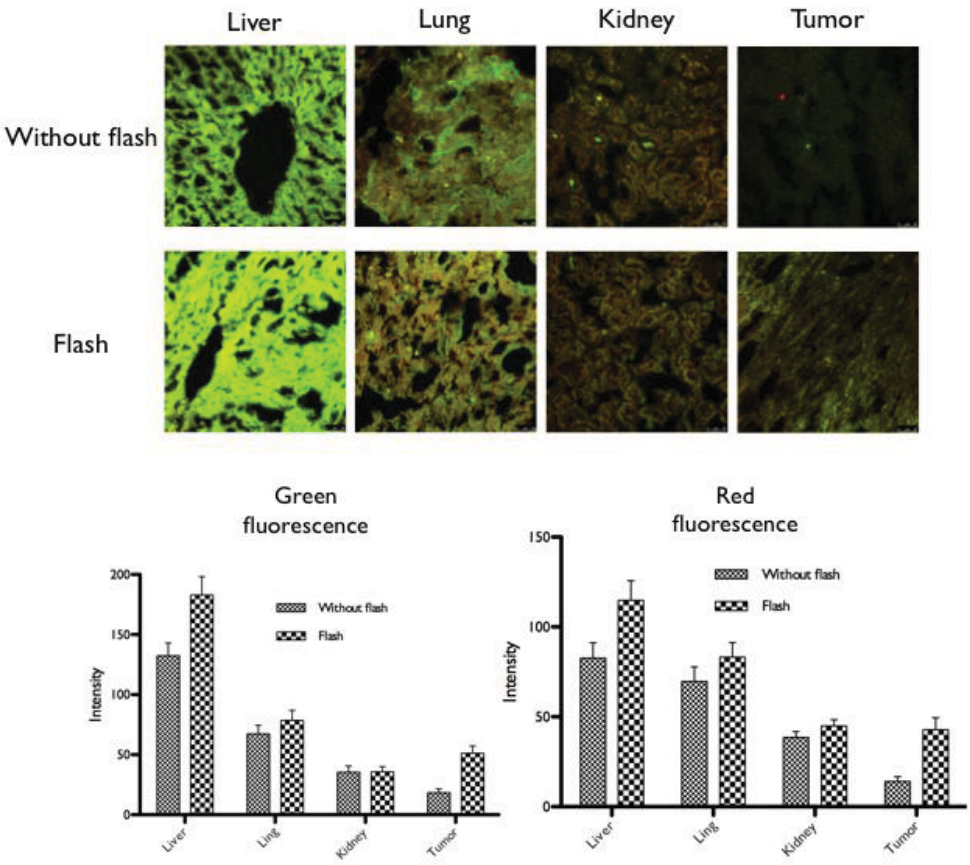

Figure 1-15. Bio-distribution of HER2-MB_G-$Lipo_R$. Bio-distribution results of HER2-MB_G-$Lipo_R$ determined by CSLM after intra-arterial (IA) injection and quantified.

1.4. Conclusions

Theranostic agents are a promising clinical application strategy for accurate, facile disease detection and treatment method. A hybrid theranostic agent for ultrasound (US) was herein reported, namely a microbubble and liposome complex (MB-Lipo) particle. Applying US for its detection as well as activation, I showed that the MB-Lipo platform has unique advantages over other theranostic modalities (e.g., photodyamic theraphy, magnetic hyperthermia). **First,** the detection modality enables real-time, deep tissue imaging, and the use of MBs significantly improves the signal contrasts. **Second,** the MB-Lipo particles can be remotely activated by the same US scanner (flash mode) during imaging; this capacity not only simplifies the required instrumentation, but also offers high spatiotemporal precision in treatment. **Third,** MB bursting with US pulses could amplify the intracellular delivery of therapeutic liposomes by temporarily increasing local cell membrane permeability (sonoporation). As a proof-of-concept, MB-Lipo particles have been synthesized and systematically characterized. Both MBs and Lipos were produced with FDA-approved phospholipids, to maximize the product' biocompatibility for in vivo applications. As a contrast agent, MB-Lipo particles yielded high US signal, similar to that of a commercial agent (SonoVue®). Enhanced drug delivery through US activation (flash pulses)

was also validated. Importantly, the particles were proven to be a versatile platform for multi-functional operation. It can be rendered highly target-specific by grafting affinity ligand, and many different types of agents (e.g., molecular drugs, genetic material) could be loaded together to enhance therapeutic efficacy. MB-Lipo particles were used to deliver plasmid DNA to cancer cells as well as to primary cells, achieving transfection efficiency higher than that of a commercial agent. The particles also showed a high efficacy in cancer detection and treatment. In an animal study, local tumor could be targeted with the particles, which was confirmed by concurrent US imaging. Subsequent application of US flash released therapeutic materials in a site-specific and time-specific manner. Such treatments, benefitting from the efficient delivery and high potency (combination of anticancer drug and therapeutic gene) of MB-Lipo particles, enabled a significant reduction in tumor burden. All these results validated the dual use of MB-Lipo particles as a US contrast agent and a therapeutic delivery vehicle. Going forward, I envision that the developed MB-Lipo particles could have broader applications. The developed technology could promote early detection and treatment response monitoring, eventually informing personalized medicine strategies. The platform could also be used in other diseases (diabetes or arteriosclerosis), wherein US imaging is already widely employed. To facilitate the MB-Lipo' clinical translation, I plan to conduct the toxicology

study as well as pre-clinical trial to evaluate its treatment efficacy[42].

1.5. References

1. Kelkar S. S., Reineke T. M., *Bioconjug. Chem.*, 22, 1879-1903 (2011).

2. Janib S. M., Moses A. S., Mackay J. A., *Adv. Drug. Deliv. Rev.*, 62, 1052-1063 (2010).

3. Ansari C., Tikhomirov G. A., Hong S. H., Falconer R. A., Loadman P. M., Gill J. H., Castaneda R., Hazard F. K., Tong L., Daldrup-Link H. E., *Small*, 10, 566-575 (2014).

4. Cho H. S., Frangioni J. V., *Mol. Imaging*, 9, 291-310 (2010).

5. Yoke R., Grulke E., MacPhail R., *Wiley Interdiscip. Rev. Nanomed. Nanobiotechnol*. 5, 346-373 (2013).

6. Yong K. T., Law W. C., Hu R., Ye L., Liu L., Swihart M. T., Prasad P. N., *Chem. Soc. Rev.*, 42, 1236-1250 (2013).

7. Al-Jamal W. T., Kostarelos K., *Acc. Chem. Res.*, 44, 1094-1104 (2011).

8. Nguyen A. T., Wrenn S. P., *Wiley Interdiscip. Rev. Nanomed. Nanobiotechnol.*, 6, 316-325 (2014).

9. Hasik M. J., Kim D. H., Howle L. E., Needham D., Prush D. P., *Ultrasonics*, 40, 973-982 (2002).

10. Akbarzabeh A., Rezaei-Sadabady R., Davaran S., Joo S. W., Zarghami N., Hanifehpour Y., *Nanoscale Res. Lett.*, 8 102-110 (2013).

11. Barenholz Y., *J. Control Release*, 160, 117-134 (2012).

12. Ferrara K., Pollard R., Borden M., *Annu. Rev. Biomed. Eng.*, 9, 415-447

(2007).

13. Sirsi S. R., Borden M. A., *Theranostics*, 2, 1208-1222 (2012).

14. Klibanov A. L., Shevchenko T. I., Raju B. I., Seip R., Chin C. T., *J. Control Release*, 148, 13-17 (2010).

15. Yan F., Li L., Deng Z., Jin Q., Chen J., Yang W., Yeh C. K., Wu J., Shandas R., Liu X., Zheng H., *J. Control Release*, 166, 246-255 (2013).

16. Mitragotri S., *Nat. Rev. Drug Discov.*, 4, 255-260 (2005).

17. Geers B., Lentacker I., Sanders N. N., Demeester J., Meairs S., De Smedt S. C., *J. Control Release*, 152, 249-256 (2011).

18. Kheirolomoom A., Dayton P. A., Lum A. F., Little E., Paoli E. E., Zheng H., Ferrara K. W., *J. Control Release*, 118, 275-284 (2007).

19. Dayton P. A., Allen J. S., Ferrara K. W., *J. Acoust. Soc. Am.*, 112, 2183-2192 (2002).

20. Prentice P., Cuschieri A., Dholakia K., Prausnitz M., Campbell P., *Nat. Phys.*, 1, 107-110 (2005).

21. Manjappa A. S., Chaudhari K. R., Venkataraju M. P., Dantuluri P., Nanda B., Sidda C., Sawant K. K., Murthy R. S., *J. Control Release*, 150, 2-22 (2011).

22. Deng C. X., Sieling F., Pan H., Cui J., *Ultrasound Med. Biol.*, 30, 519-526 (2004).

23. Chang I. S., Lee M. W., Kim Y. I., Choi S. H., Kim H. C., Choi Y. W.,

Yoon C. J., Shin S. W., Lim H. K., *J. Vasc. Interv. Radiol.*, 22, 1181-1187 (2011).

24. Ninomiya H., *Anat. Histol. Embryol.*, 29, 301-305 (2000).

25. Delalande A., Kotopoulis S., Postema M., Midoux P., Pichon C., *Gene*, 525, 191-199 (2013).

26. Noble M. L., Kuhr C. S., Graves S. S., Loeb K. R., Sun S. S., Keilman G. W., *Mol. Ther.*, 21, 1687-1694 (2013).

27. Zhou Y., Kumon R. E., Cui J., Deng C. X., *Ultrasound Med. Biol.*, 35, 1756-1760 (2009).

28. Arangoa M. A., Düzgünes N., Tros de llarduya C., *Gene Ther.*, 10, 5-14 (2003).

29. Inho Y., Furuno T., Hirashima N., Kitamoto D., Nakanishi M., *Eur. J. Pharm. Sci.*, 49, 1-9 (2013).

30. Gabizon A., Shmeeda H., Grenader T., *Eur. J. Pharm. Sci.*, 45, 388-398 (2012).

31. Haran G., Cohen R., Bar L. K., Barenholz Y., *Biochim. Biophys. Acta.*, 1151, 201-215 (1993).

32. Lee C., Dhillon J., Wang M. Y., Gao Y., Hu K., Park E., Astanehe A., Hung M. C., Eirew P., Eaves C. J., Dunn S. E., *Cancer Res.*, 68, 8661-8666 (2008).

33. Kang Y., Park M. A., Heo S. W., Park S. Y., Kang K. W., Park P. H., Kim J.

A., *Biochim. Biophys. Acta.*, 1830, 2638-2648 (2013).

34. Choi Y. J., Li X., Hydbring P., Sanda T., Stefano J., Christie A. L., Signoretti S., Look A. T., Sicinski P., *Cancer Cell*, 22, 438-451 (2012).

35. Dubik D., Dembinski T. C., Shiu R. P., *Cancer Res.*, 47, 6517-6521 (1987).

36. Stennicke H. R., Salvesen G. S., J. *Biol. Chem.*, 272, 25719-2523 (1997).

37. Sabine V. S., Faratian D., Kirkegaard-Clausen T., Bartlett J. M., *Histopathology*, 60, 369-371 (2012).

38. Luo W., Zhou X., Zheng X., He G., Yu M., Li Q., *J. Ultrasound Med.*, 29, 51-60 (2010).

39. Prabhakar U., Maeda H., Jain R. K., et al., *Cancer Res.*, 73, 2412-2427 (2013).

40. Chow E. K., Ho D., *Sci. Transl. Med.*, 5, 216-224 (2013).

41. Bertrand N., Wu J., Farokhzad O. C., *Adv. Drug Deliv. Rev.*, 66, 2-25 (2014).

42. Yoon Y. I., Kwon Y. S., Cho H. S., Heo S. H, Park K. S., Park S. G., Lee S. H., Hwang S. I., Kim Y. I., Jae H. J., Ahn G. J., Cho Y. S., Lee Hakho, Lee H. J., Yoon T. J., *Theranostics*, 4, 1133-1144 (2014).

Chapter 2

Particles for the ultrasound/MRI dual imaging and theranostics applications

2.1. Introduction

One of the major advantages of theranostic materials is their ability to simultaneously perform multiple functions. A single particle can be used to diagnose a disease and to image cells.[1-3] To date, most of the organic, inorganic, and compound theranostic agents developed contain polymer particles, magnetic nanoparticles, quantum dots, and novel metal substrates. While these theranostic agents exhibit multiple attractive properties, namely enhanced bio-availability with prolonged circulation time, preferential tumor accumulation owing to the enhanced permeability and retention (EPR) effect and imaging compatibility with existing detection modalities (e.g., magnetic resonance imaging or optical excitation), their clinical translation remains challenging.[4-7] The potential toxicity of the constituent materials (especially the inorganic nanoparticles) raises significant safety concerns and toxicological evidence, all of which need to be carefully addressed prior to their clinical applications.[8-10]

Microbubbles (micro-meter sized bubble, MBs) and liposomes (Lipos) are emerging biocompatible materials for cancer diagnosis and treatment, and therefore represent a safer alternative to conventional theranostic agents.[11, 12] By coupling MBs and Lipos as a complex, this concept material has been shown to achieve simultaneous ultrasound (US) imaging of cells as well as

highly efficient targeted delivery of therapeutic loads.[13, 14] Moreover, when integrated with super-paramagnetic iron-oxide nanoparticles, the assembly provided dual contrast in both magnetic resonance (MR) and US imaging.[15] While such formulation enabled multi-model imaging, the incorporation of inorganic particles reduces its biocompatibility and limits its clinical potential, as with conventional theranostic agents.

Herein, we report the preparation of a fully biocompatible and multifunctional hybrid complex comprising of MB, Lipo, and Fe^{3+} ion-chelated melanin nanoparticles (MNPs) that can enable dual US-MR imaging as well as enhanced gene delivery. Leveraging on the high Fe^{3+} loading capacity of MNPs, the resultant complex achieves MR contrast from only biocompatible chemicals.[16] The resulting complex particles generated high contrast under normal US illumination, as MBs oscillated and generated acoustic waves. For the delivery of therapeutic materials, we burst MBs in situ by applying higher acoustical pressure (US flash); this unloaded Lipos and MNPs from MBs as well as the temporarily permeabilized cellular membrane for efficient delivery.[17, 18] We further functionalized the complex particles with antibody and showed (1) specific targeting to tumor cells and (2) US-stimulated effective delivery of the linked MNPs and Lipos into the cells. After localized application of moderate to high acoustic pressure, we observed enhancements in both the MRI signal as well as the therapeutic effect by the

internalized MNP and Lipo particles.

2.2. Experimental Section

2.2.1. Preparation of MB, Lipo, MNP (Fe), and their complexes

1,2-Dipalmitoyl-sn-glycero-3-phosphatidylcholine (DPPC, 15.4 mg), diacetyl phosphate (DCP, 1.0 mg), 1,2-dipalmitoyl-sn-glycero-3-phosphoethanolamine (DPPE, 1.2 mg), 1,2-distearoyl-sn-phosphoethanolamine-N-[PDP(polyethylene glycol)-2000] (DSPE-PEG-PDP, 5.0 mg), and cholesterol (3.5 mg) were dissolved in 5 mL chloroform (99.9 %, Sigma-Aldrich, St. Louis, MO, USA). The mixed solution was allowed to evaporate for 5 min at room temperature and was then freeze-dried for 24 h at -45 °C to induce the formation of a phospholipid film. Subsequently, 2 mL of a solution containing glycerin, propylene, and H_2O (volume ratio: 1:2:7) was added to the film and the solution was gently shaken. It was then transferred to a hermetic vial (Wheaton, NJ, USA) and vigorously mixed for 15 s with a mechanical high-speed shaking-device (KIMS, South Korea) during bubbling with SF_6 gas. The prepared MB particle solution was stored in a refrigerator. Lipo was produced from a chloroform solution containing DPPC, DCP, DPPE, and cholesterol. The solution was evaporated and lyophilized as above. After adding 2 mL H_2O, the lipid film underwent sonication for 5 min at 60 °C. The solution was subjected to a freeze-thaw cycle five times, using liquid nitrogen

and a water bath. The prepared Lipo dispersion solution was extruded through a 200 nm filter at 60 °C (mini-extruder, Avanti polar lipids). To render green and red fluorescence, fluorescein isothiocyanate (1 mg, Sigma-Aldrich) and Texas red (1 mg, Sigma-Aldrich) were homogeneously added to the lipid mixed solution before generating a film of MB and Lipo, respectively. The excess organic dyes were continually removed by centrifugation (5 min at 13,000 rpm) and washing with H_2O, until the color of the supernatant disappeared completely. To fabricate the sulfhydryl functional groups on the Lipo, 2 mL amine active Lipo (21 mg), derived from DPPE, was reacted with 5 mg of 2-iminothiolane·HCl (Traut' reagent, Pierce) for 2 h at room temperature, after adjusting the pH to 8.2 with 1 M $NaHCO_3$. The 2 mL thiolated Lipo (10.5 mg/mL) and 1.5 mL MB (13.1 mg/mL) solutions were gently shaken for 2 h at room temperature and the complex reaction was monitored through calculating of the amounts of pyridine-2-thione in supernatant by UV-Vis spectroscopy. To prepare the MNP particles, 180 mg of dopamine hydrochloride was dissolved in distilled water at 50 °C and 780 μL of NaOH solution (1 M) was vigorously stirred. After 6 h, the color turned black and the solution was centrifuged (10 min at 20,000 rpm), and washed several times with distilled water. The MNP particles displayed a characteristic size (diameter ~ 100 nm), and showed uniform size distribution, as determined by TEM and DLS. In order to coordinate the Fe^{3+} ion, 4 mL of

$Fe(NO_3)_3 \cdot 6H_2O$ with the concentration range (2-10 μmol) was mixed with 10 mL of the MNP dispersion solution (1 mg/mL). After stirring for 3 h, the solutions were centrifuged (10 min at 20,000 rpm), and the unbound Fe^{3+} ions in the supernatant solution were quantitatively estimated in order to determine the overall loading capacity. This was achieved with an inductively coupled plasma atomic emission spectrometer (ICP-AES). The thiolated MB-Lipo (called ML) complex solution (30 mg, 15 mg/mL) was homogeneously mixed with 1 mL of the MNP (Fe) solution (1 mg/mL) for 0.5 h at room temperature. The excess MNP (Fe) were removed by centrifugation (5 min at 13,000 rpm) and by washing the ML-MNP (Fe) complexes trice with distilled water. To increase the stability in aqueous environments, the resulting complex particle solution was treated with 2 mL of methoxypoly(ethylene glycol) (PEG-SH, 2 kD, 0.5 mM) for 1 h at room temperature and the excess PEG-SH was removed by centrifugation (2 min at 13,000 rpm). The size and shape of the complex was characterized using SEM, TEM, and DLS measurements. In our preparation, all phospholipid chemicals were purchased from Avanti Polar Lipids and all other chemical reagents were purchased from Sigma-Aldrich. All chemicals were used without further purification.

2.2.2. HER2 antibody conjugation

In order to fabricate with an active maleimide functional group, 2 mL of the ML-MNP(Fe) particle solution (14.9 mg/mL) containing an amine functional group was reacted with sulfosuccinimidyl-4-(N-maleimidomethyl) cyclohexane-1-carboxylate (Sulfo-SMCC, 5 mg, Sigma-Aldrich) for 3 h, after adjusting the pH to 8.2 with a 1 M $NaHCO_3$ solution. The maleimide moiety was then linked to the appropriate HER2 half antibody using a general bio-conjugation procedure. The antibody-harboring particles were quantitatively analyzed using a typical protein estimation assay.

2.2.3. Cell toxicity assay

A 3-(4,5-dimethylthiazol-2-yl)-2,5-diphenyltetrazolium (MTT) assay kit (Invitrogen) was utilized to evaluate the cell viability in the presence of the ML-MNP(Fe) particles. The SKBR3 cells (ATCC, VA, USA) were cultured in RPMI supplemented with 10 % FBS, penicillin, and 1% streptomycin. Cells were maintained at 37 °C in a 5 % CO_2 incubator. The cells were washed, trypsinized, and re-suspended in the culture medium after they achieved the desired 80 % confluence. The cells were then seeded at a concentration of 5,000 cells/well in a 96-well tissue culture plate and allowed to grow overnight in a CO_2 incubator. Various concentrations of the ML-MNP (Fe) in 1 mL PBS buffer solution were added to cell culture solution and the cells

were allowed to grow for another 24, 48, and 72 h, respectively. To determine the cell viability, the culture medium was replaced with an MTT solution. After 3 h of incubation inside a CO_2 incubator, the MTT solution was added to dissolve the resulting formazan crystals. The cell viability was determined spectrophotometrically at 570 nm, with a background subtraction at 690 nm.

2.2.4. US phantom study

The echogenicity of HER2-ML-MNP (Fe) was evaluated using a phantom sample. This solution was made using a plastic connecting tube with an inner diameter of 2 mm, located in a chamber filled with water. 9 mg of the particles or SonoVue® solution in 2 mL PBS were passed through the plastic tube at 0.1 mL s^{-1}. An ultrasound scanner (iU22, Philips, Bothell, WA, USA) equipped with a 5-12 MHz broadband linear probe was used for imaging (Mechanical Index, MI : 0.08).

2.2.5. Phantom and in vitro MR study

For a T_1 weighted (T_1-w) MR phantom study, various concentrations (0-1000 nM, [Fe] or [Gd]) of HER2-ML-MNP (Fe) or Gadovist® were prepared by fusing these into a 0.5 % agarose gel (1:1 volume ratio). To test in vitro

MR imaging, a 3 μM [Fe] concentration of the particles were incubated with HER2-positive SkBr3 and HER2-negative MCF7 cells for 1 h inside a 5 % CO_2 incubator. Subsequently, a US probe was placed in the backside of the well plate and 6 flash pulses (MI : 0.61) were applied for 1 min. The excess particles were removed by washing the cell culture with the culture media, and the treated cells were detached by trypsinization and subsequently centrifuged at 3,000 rpm. All T_1-w MR images were acquired on a 3.0-T clinical MR scanner (Philips medical system, Netherland, archieva Release 3.2.1.0 version). Axial and coronal T_1-w images were obtained with a TR 400 ms, a TE 10 ms, a 240 × 240 matrix, a flip angle 90 degrees, a slice thickness 3 mm, number of averages with 4, bandwidth 115 Hz/pixel and the FOV of 120 × 120 mm.

2.2.6. siSurv incorporation and cell treatment

To prepare Protamine (PA, 7.5 kD) and siRNA complex, the siSurv gene (50 μM) and different concentration of PA solutions (10-80 μM) were incubated for 1 h at room temperature using plate shaker. And it was optimized that the ratio of PA and siSurv concentration was 40 and 50 μM, respectively. To generate liposome incorporation, the fresh PA and siSurv complex solution was homogenized into Lipo powder (21 mg, 2 mL) for 5

min at room temperature, using electrophoresis. The Lipo-harboring siSurv-PA was washed twice with centrifugation (5 min at 13,000 rpm) to remove the unloaded gene complex and the loading capacity was then estimated with a UV-vis spectrophotometer. The 10.5 mg $Lipo_{siSurv}$ dissolved in 1 mL aqueous solution was reacted with Traut's agent (5 mg) for thiolation of DPPE and sulfhydryl terminated Lipo complex were mixed with thiol active MB 1 mL aqueous solution (13 mg). And the ML_{siSurv} solution was progressed to MNP (Fe) and antibody conjugation according to above particle preparation procedure. Subsequently, 3×10^4 cells were seeded onto a 48-well plate (BD Falcon) and HER2-ML_{siSurv}-MNP (Fe) (1 mg) in 0.5 mL PBS were added to the cells in the culture medium containing 10 % FBS. Following 1 h of incubation, the excess particles were washed out with a PBS solution. For flash application, the clinical US scanner probe was placed at the back of the 48-well plate and flash pulses (MI : 0.61) were applied for 1 min. The treated cells were also washed twice with the culture medium, and then subcultured for 2 days.

2.3. Results and Discussion

2.3.1. Preparation of functional HER2-ML-MNP (Fe) complex

Scheme 2-1 demonstrated preparation process of the HER2-ML-MNP (Fe) complex. The HER2-ML-MNP (Fe) complexes were synthesized by a three-step chemical reaction; an MB-Lipo hybrid reaction, MNP (Fe) anchoring, and antibody conjugation (scheme 2-1). For the ML preparation (scheme 2-1-i), DSPE-PEG-SPDP in MB was cross-linked with the sulfhydryl groups after the thiolation of Lipo-DPPE, and the complete hybrid reaction was confirmed by the detection of pyridine-2-thione as a leaving chemical group with a UV-vis spectrometer. MNP (Fe) was attached to the thiolated Lipo (scheme 2-1-ii), which was further treated with HS-PEG chemicals in order to increase the solubility in aqueous environments. Finally, to render specificity to the complexes, the HER2 half antibody (HER2) was bound to the maleimide functional group on the MB and Lipo after reaction of the Sulfo-SMCC with DPPE (scheme 2-1-iii). Figure 2-1 elucidated characterization of MBs, Lipos and MNP (Fe)s. The spherical shape of the MBs and Lipos was confirmed with a microscope (Fig. 2-1b) and a cryo-transmission electron microscope (cryo-TEM) (Fig. 2-1a). The synthesized MBs and Lipos were spherical, with an average diameter of ~ 1.3 mm and ~ 200 nm, respectively. The resulting

spherical MNP had an average diameter of ~ 100 nm and a regular size distribution. Fe^{3+} ion chelated MNP, MNP (Fe) showed a spherical shape, as evident from the TEM analysis (Fig. 2-1c) and the intensity of the iron metal bound to the MNP surface (Fig. 2-1c, inset) was mapped by scanning transmission electron microscopy (STEM) (Fig. 2-1c, right-up). The qualification analysis was also conducted with STEM equipped with EDX, and several energy-dispersed peaks indicated the presence of iron metal (Fig. 2-1c, right-bottom, relevant peaks are marked with red arrows). MNPs were chelated with Fe^{3+} ions onto the o-dihydroxyl group of the catechol unit on the MNP surface.

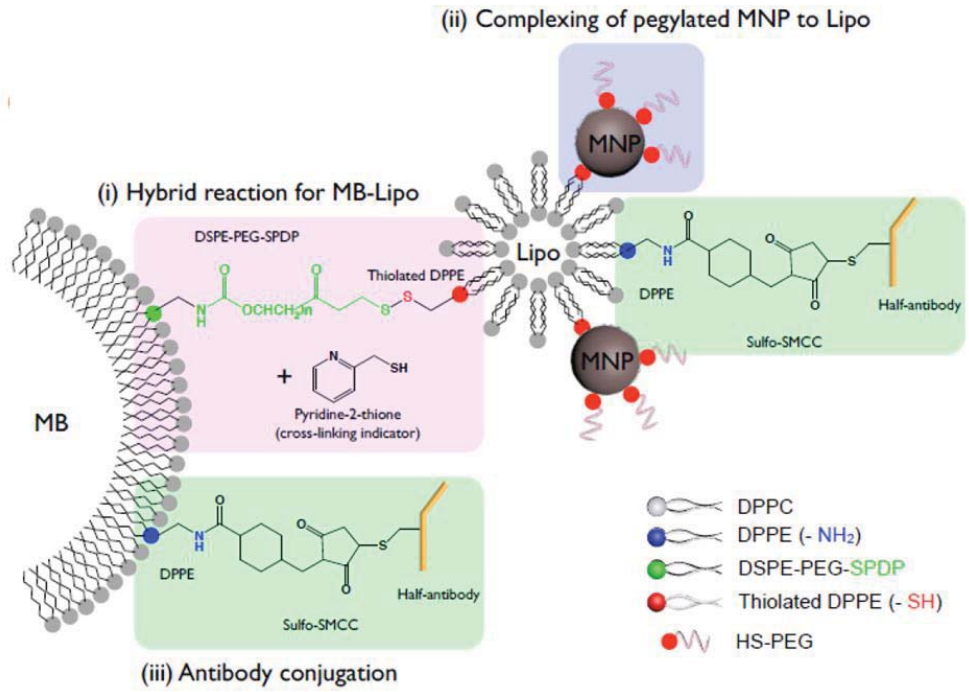

Scheme 2-1. Synthetic procedure to prepare the functional HER2-ML-MNP (Fe) complex.

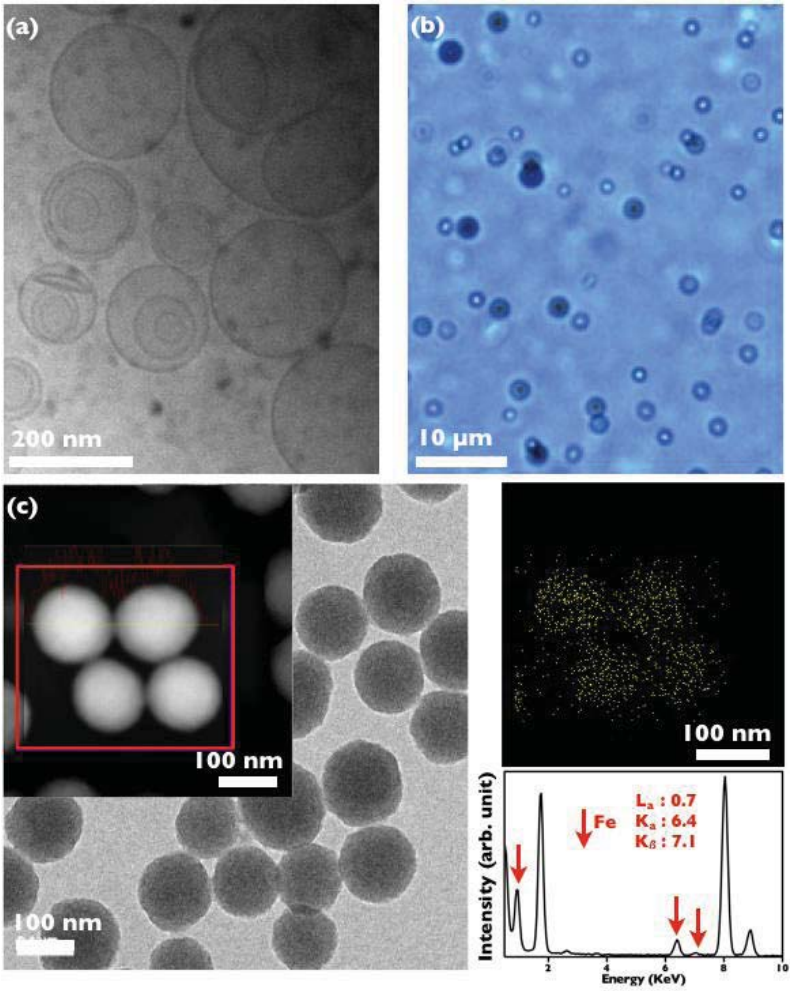

Figure 2-1. Characterization of MB, Lipo, and MNP (Fe). Microscope images of MBs (a) and cryo-TEM images of Lipo (b). STEM images of MNP (Fe).

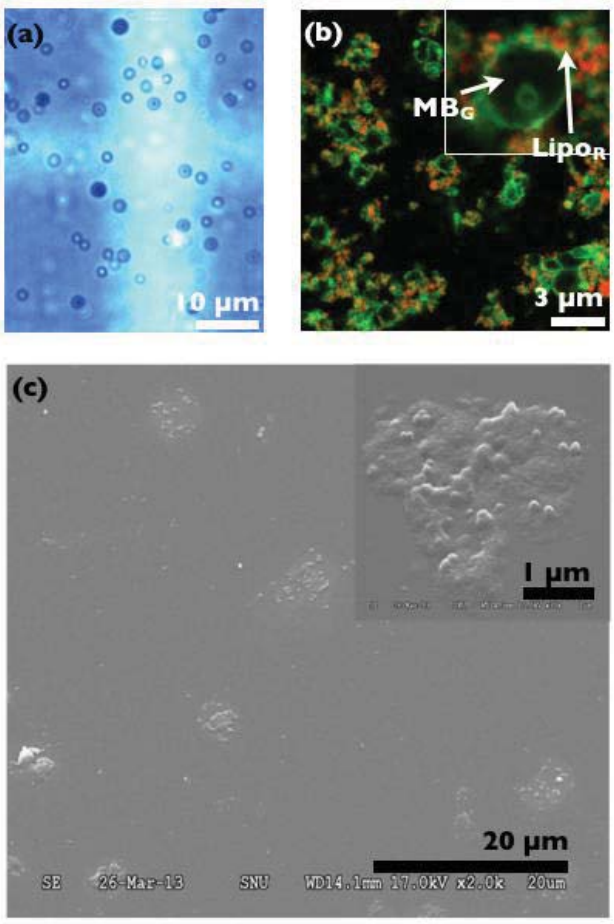

Figure 2-2. Characterization of HER2-M_GL_R-MNP (Fe). Microscope (a), CLSM (b), and SEM images of HER2-M_GL_R–MNP (Fe) (c).

The HER2-M_GL_R-MNP (Fe) was characterized the shape by optical microscope (Fig. 2-2a). After all synthetic procedures, the morphology of the complex was maintained. The MB and Lipo cores comprise of a hydrophobic gas phase and a hydrophilic aqueous phase, respectively. During the preparation, I also added a hydrophobic dye (fluorescein isothiocyanate, G) for localizing the alkyl chain of the MB shell, and a red hydrophilic dye (Texas Red, R) for incorporation into the aqueous Lipo core (Fig. 2-2b). The red and green organic dyes incorporated into the Lipo and MB complexes were characterized with a confocal laser scanning microscope. The MB revealed a hollow sphere due to the core SF_6 gas, and the Lipos around the green MB were indicated by small red dots (Fig. 2-2b, inset). Scanning electron microscope (SEM) results explained ML complex was bound with MNP (Fe) (Fig. 2-2c). There were rarely MNPs (Fe) seperated from ML complexes.

The average diameter of the ML was approximately 1.6 μm. Subsequently, the synthesized MNP (Fe) was attached onto the excess sulfhydryl moiety present on the Lipo of the ML complex, via a Schiff's base or a Michael addition reaction.[19] The ML-MNP (Fe) complexes were treated with methoxy-poly(ethylene glycol) (PEG-SH, 2 kDa) to increase their solubility in aqueous buffers. For specific cancer cell targeting by the ML-MNP (Fe) complexes, an antibody against human epidermal growth factor receptor 2 (HER2) was

introduced to the particles by a typical half-antibody conjugation procedure, and the anchored antibodies were quantitatively analyzed by a protein determination method (not shown, 70 nM HER2 antibody per mM DPPC of the particle).[20, 21]

The size of the synthesized materials slightly increased according to reaction steps (Fig. 2-3). These results showed that the synthesized products were prepared as designed.

To test the chelating capacity of Fe^{3+} ions onto the melanin nanoparticle (MNP), $Fe(NO_3)_3 \cdot 6H_2O$ was dissolved in distilled H_2O at various concentrations (2-10 μmol), and then mixed with 1 mL of the solution with dispersed MNPs (1 mg/mL). The amount of loaded Fe^{3+} ions was determined directly by ICP-AES analysis (Fig. 2-4a). Fe^{3+} ions were maximized to ~ 3 μmol loading capacity per mg of MNP, while treating with 8 μmol of Fe^{3+} ion solution. More importantly, the chelated Fe^{3+} ions should not release from the MNP at various pH levels that meant sustaining ability for a contrast agent. An extremely low amount of Fe^{3+} ions was detected (< 5 %) after 3 days of stirring at various pH levels (4, 7, and 10), according to the ICP-AES analysis (Fig. 2-4b). These results indicated that MNP (Fe) had good safety to avoid side effects further in vitro study.

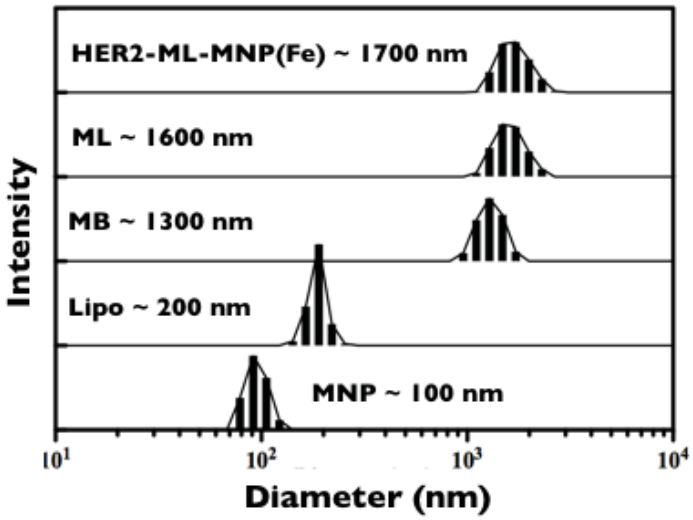

Figure 2-3. DLS results of MNPs, Lipos, MBs, MLs, and HER2-ML-MNP (Fe) complexes.

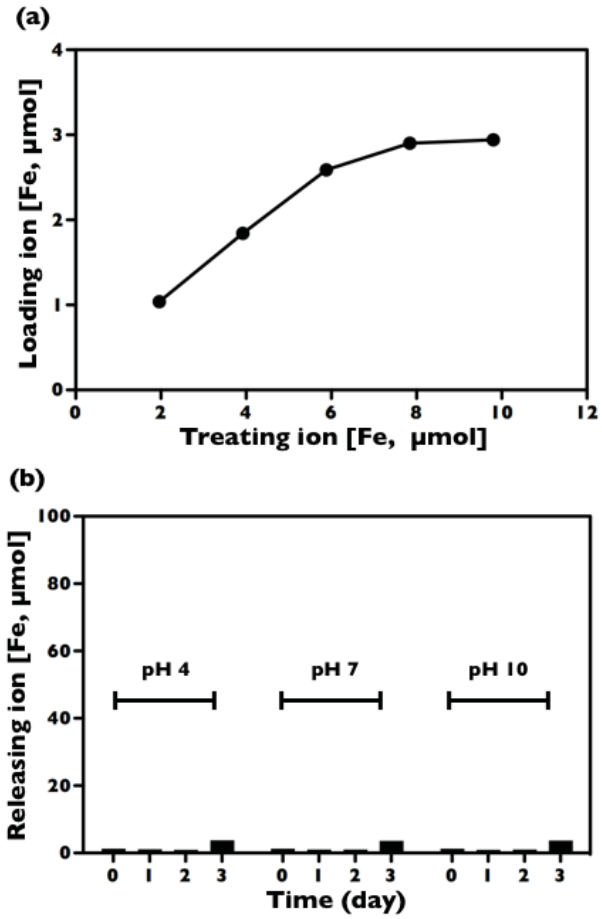

Figure 2-4. Chelating capacity (a) of Fe^{3+} ions onto the MNP by ICP-AES and releasing test (b) of chelated Fe^{3+} on the MNP at various pH and for 3 days.

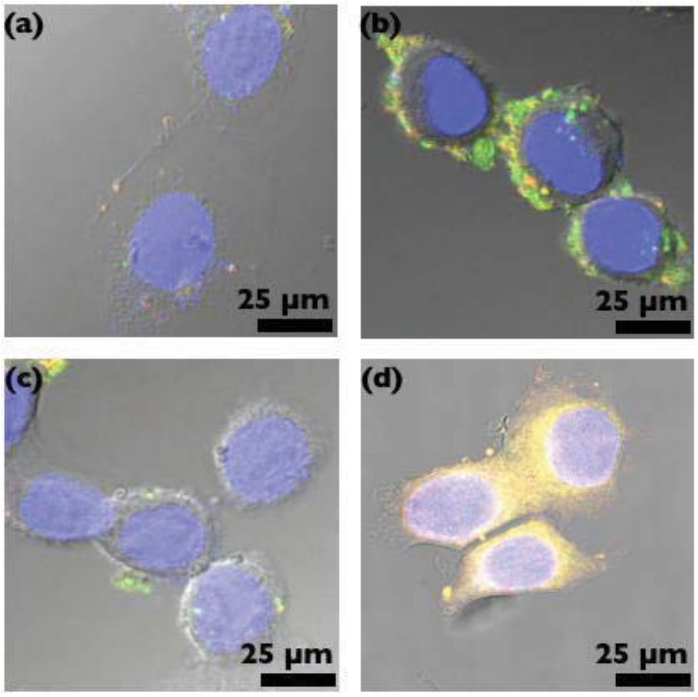

Figure 2-5. Characterization of cancer cells treated by fluorescent complexes. CLSM results of MCF7 (a) and SkBr3 (b) treated by HER2-M_GL_R-MNP (Fe). CLSM results of SkBr3 treated by M_GL_R-MNP (Fe) (c) or HER2-M_GL_R-MNP (Fe) (d) with US flash treatment.

2.3.2. Cancer cell targeting and enhanced intracellular delivery

To investigate the specific targeting ability and uptake enhancement by US stimulation, the prepared particles were incubated with breast cancer cells (Fig. 2-5). The cells were treated with HER2-M_GL_R-MN P(Fe)-HER2 solution (1 mL, 0.33 mg/mL PBS buffer) for 1 h at 37 ^oC inside a 5% CO_2 incubator. Green and red fluorescent HER2-M_GL_R-MNP (Fe) recognized the Her2 receptor highly expressed in breast cancer cells (SkBr3) compared with negative cells (MCF7, Fig.2-5a, the blue color indicates the DAPI-stained nucleus). The HER2 conjugated complexes were present on the cell membranes (Fig. 2-5b). The non-antibody conjugated M_GL_R-MNP (Fe) treated SkBr3 cells rarely showed fluorescence (Fig. 2-5c) after exposure to US flash (MI : 0.61). But HER2-M_GL_R-MNP (Fe) treated SkBr3 cells with US flash exhibited the meaningful fluorescent intensity into the cell cytosol (Fig. 2-5d). During the treatment, the complexes adhered just to the cell membrane and not penetrated into the cytoplasm due to the large-sized MBs. However, the HER2-M_GL_R-MNP (Fe) could be exploited to significantly improve the delivery of Lipos and MNPs (Fe) into cells; burst of MBs at the flash mode not only released the attached Lipos and MNPs (Fe), but also enhanced the permeability of the cell membrane (sonoporation) for more efficient particle uptake.[22] Enhancement of the uptake efficiency via specific targeting based

US flash illumination was illustrated (Fig. 2-6). HER2-ML-MNP (Fe) can exhibit specific targeting effect to HER2 positive SkBr3 and attach onto these cells. After US flash (MI : 0.61) for 1 min, the MB of the complex was quickly destroyed and it released the Lipo- and MNP (Fe)-linked materials into the cell. Furthermore, the destructive forces of the MB introduced pores (~ 220 nm in diameter) into the cell membrane, which eventually soaked up the linked material (Fig. 2-6a, b). Effective uptake of MNP (Fe) into SkBr3 was analyzed by bio-TEM. As a control, MCF7 cells expressing very low levels of the HER2 receptor were treated with the complexes under the same condition. The rare MNPs (Fe) were found into the cell cytosol owing to non-specific endocytosis (Fig. 2-7a, b).[23] The green and red fluorescent organic dyes from MB and Lipo that were located cytosol after exposing flash were quantitatively analyzed using FACS (Fig. 2-6c, 7c). In the case of SkBr3, higher intensity was observed.

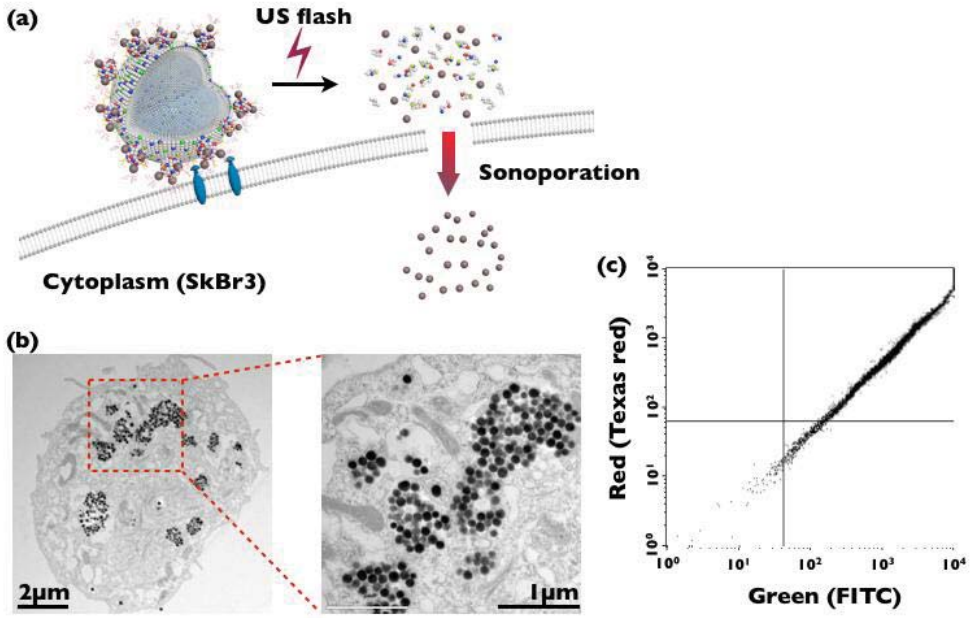

Figure 2-6. Enhancement of the uptake efficiency via specific targeting based US flash illumination. Scheme (a), bio-TEM (b), and FACS (c) results of SkBr3 treated by HER2-M_GL_R-MNP (Fe) with US flash.

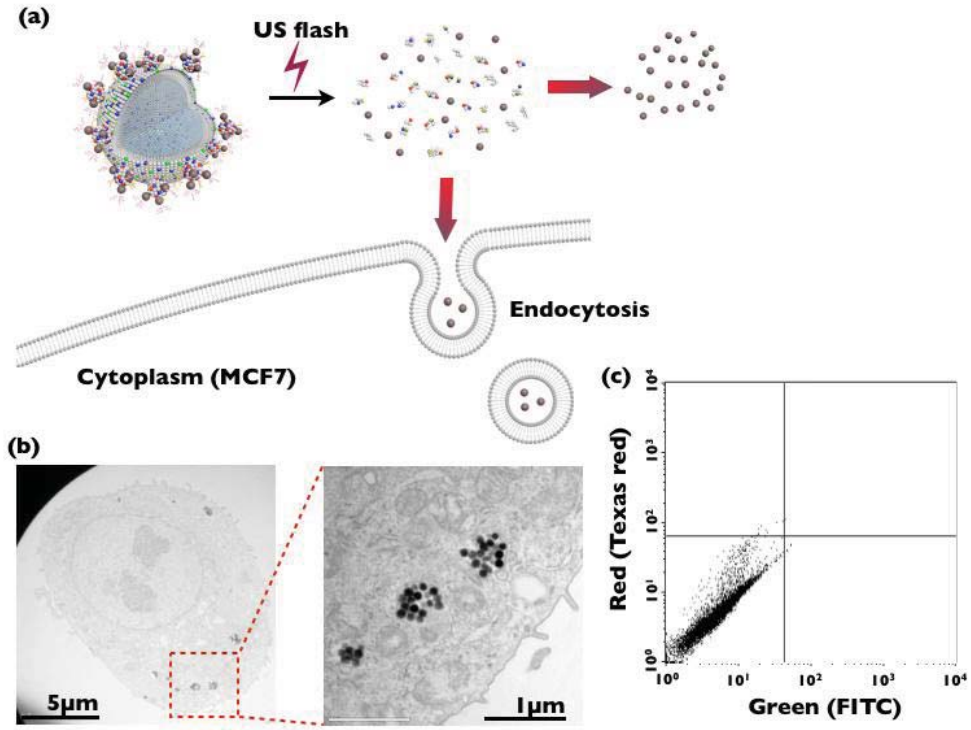

Figure 2-7. Enhancement of the uptake efficiency via specific targeting based US flash illumination. Scheme (a), bio-TEM (b), and FACS (c) results of MCF7 treated by HER2-M_GL_R-MNP (Fe) with US flash.

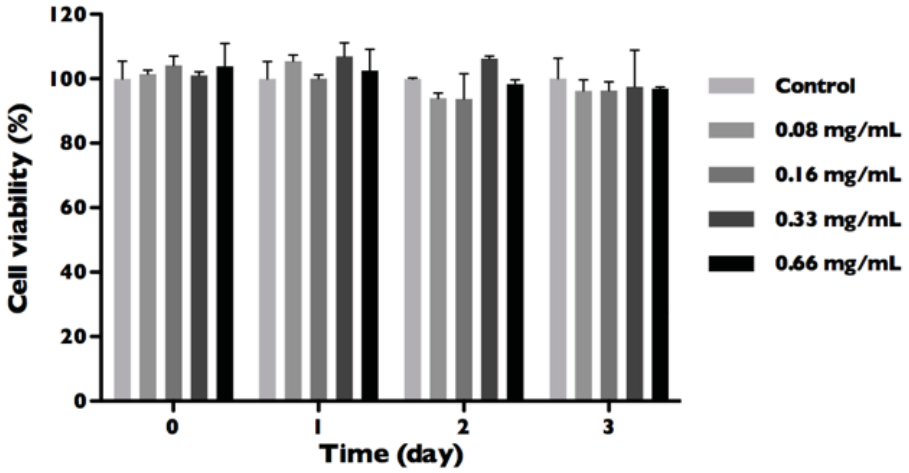

Figure 2-8. In vitro cytotoxicity assay of HER2-ML-MNP (Fe). Cell viability of SkBr3 treated by the complex of various concentrations (0-0.66 mg/mL) and US flash.

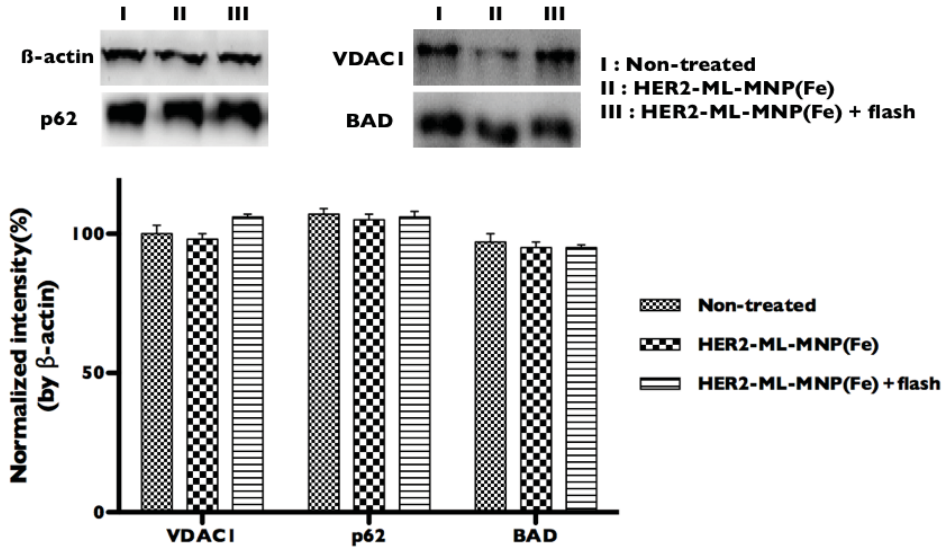

Figure 2-9. In vitro cytotoxicity assay of HER2-ML-MNP (Fe). Western blotting results of SkBr3 treated by the complex of the concentration (0.66 mg/mL) and US flash.

2.3.5. In vitro cytotoxicity assay

The cell viability after targeting and flash treatment was determined using a typical cell proliferation assay (3-(4,5-dimethylthiazol- 2-yl)-2,5-diphenyltetrazolium bromide, MTT), where we measured the effects of complex concentration and incubation time. HER2-ML-MNP (Fe) and US flash treated-cells showed a viability > 90 % (Fig. 2-8). I further investigated the biocompatibility of the complex through an assessment of cellular organelle functions [e.g., the voltage-dependent anion channel, (VDAC; mitochondria function-related protein), Nucleoporin p62 (a protein complex associated with the nuclear envelope), and the anti-apoptotic protein BAD (Bcl-2-associated death promoter)] (Fig. 2-9). All markers elicited similar expression levels in the treated and the non-treated control cells, and the US flash stimulation did not cause any cytotoxicity or functional abnormality. (All experiments were performed in triplicate)

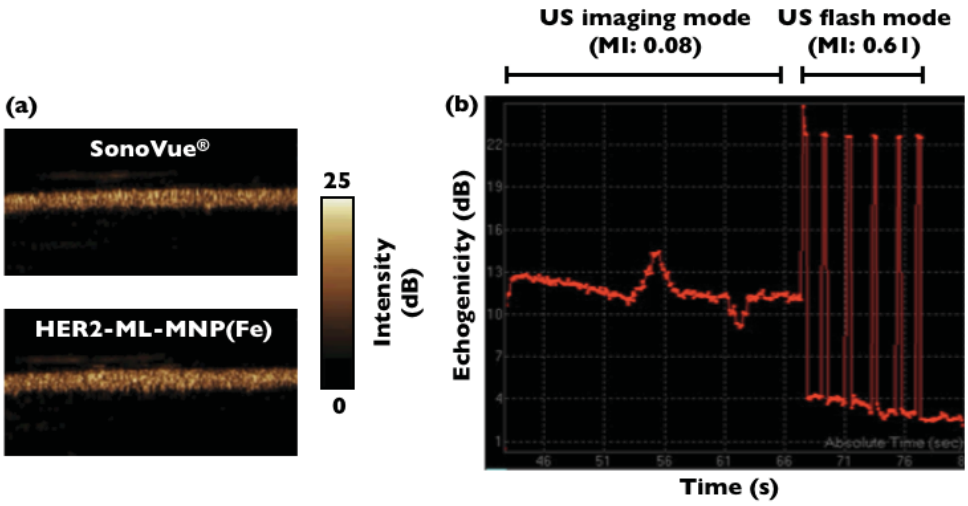

Figure 2-10. US phantom study for the comparison of echogenicity of contrast agents (a) and monitoring of MB cavitation under US flash (b).

2.3.6. In phantom study of HER2-ML-MNP (Fe) as dual US-MR contrast agents

After loading the US phantom plastic-tubes, the synthesized HER2-ML-MNP (Fe) displayed an echogenicity and intensity similar to that of a clinically used US contrast agent (SonoVue®) at the same concentration of phospholipids (DPPC, 10.5 mM) under the US imaging mode (MI : 0.08) (Fig. 2-10a, b left). The echogenicity disappeared gradually after US flash application (MI : 0.61) (Fig. 2-10b right). I found that the prepared complexes were destroyed within 6 flash treatments. The longitudinal relaxivity (r_1) value of the prepared HER2-ML-MNP (Fe) and a clinically used T_1 MR agent (Gadovist®) using a 0.47-T magnetic relaxometer (mq20, Bruker) was compared (Fig. 2-11a). The longitudinal relaxation times were measured at various concentrations of the metal ion, which was also calculated accurately using ICP-AES analysis. The complex solution showed a 2-fold higher r_1 than Gadovist. According to the Solomon-Bloembergen-Morgan (SBM) theory, a second-sphere of water molecules and oxygen atoms in the Fe^{3+} chelated catechol complexes increases r_1, and the nanoparticulate character of MNPs exhibits an enhanced r_1 and a restricted rotational mobility. For the MR phantom study with a clinically used MRI instrument (3.0-T, Philips), HER2-ML-MNP (Fe) solution had approximately 2-fold higher white contrast

intensity at the same metal ion concentration (Fig. 2-11b).

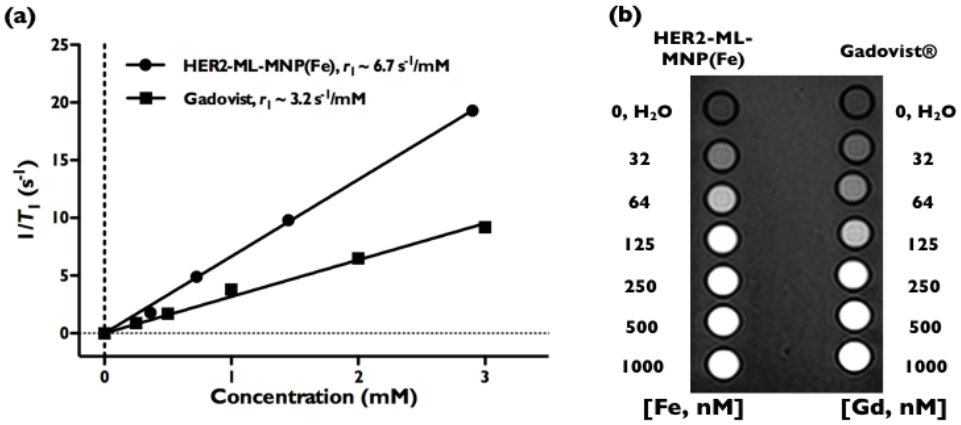

Figure 2-11. Measurement of the longitudinal relaxivity (r_1) (a) and T_1-w MR in the phantom study (b).

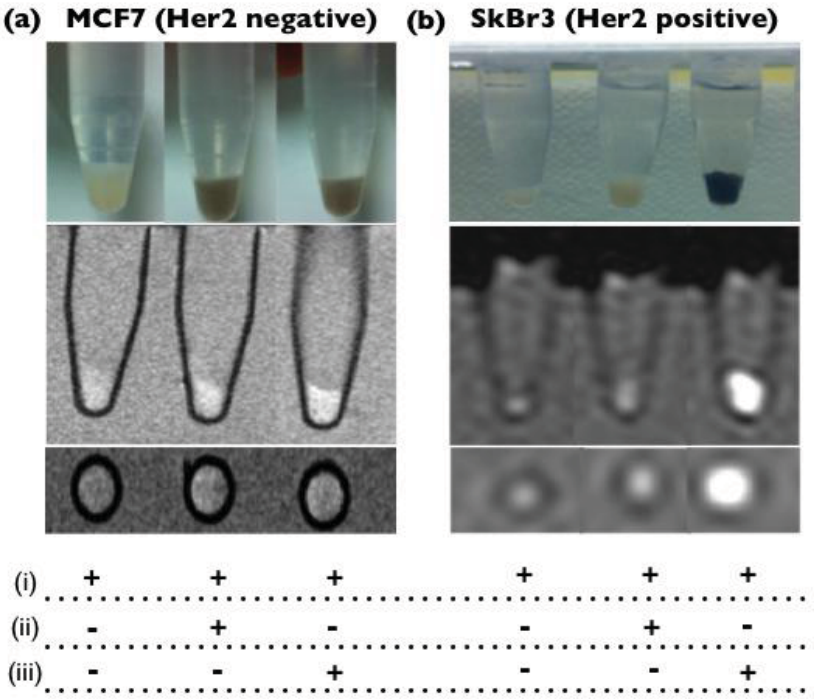

Figure 2-12. Photograph and MR imaging of targeted cells and the effect of flash stimulation. (i: flash, ii: HER2-MNP (Fe), iii: HER2-ML-MNP (Fe))

2.3.7. In vitro study of HER2-ML-MNP (Fe) as theranostic contrast agents

To monitor the US flash-mediated enhancement of T_1-w MR imaging, the HER2 positive (SkBr3) and negative (MCF7) cells underwent complexes targeting (Fig. 2-12), flash exposure (1 min), and residue removal. The treated cells were used for MR imaging (3.0 T, Philips). The flash-treated cells (in the absence of complex treatment) showed the lowest T_1-w MR signal regardless of their HER2 expression. The HER2-MNP (Fe) (without the ML complex) elicited a low signal as well, indicating that the antibody-conjugated MNP (Fe) were not sufficient to increase the MR imaging efficiency by themselves. However, HER2-ML-MNP (Fe)- and flash-treated SkBr3 cells revealed a remarkably high contrast image that might be due to increased internalization of complexes owing to the sonoporation effect. (Fig. 2-12a, b, i: flash, ii: HER2-MNP (Fe), iii: HER2-ML-MNP (Fe)). The gene for Survivin (siSurv) is a well-known therapeutic gene, which triggers cell apoptosis; the siRNA for Survivin (siSurv, 19-mer, Thermo-scientific) can be incorporated inside the Lipos.[24] To incorporate the therapeutic gene, firstly siSurv was blended with protamine (PA) through an electrostatic interaction between the two. The siSurv solution of the fixed concentration (50 μM) was added into the PA solution of the various concentrations (10-80 μM). If a surplus of siSurv is

after the conjugation reaction, the ratio is not optimized. The optimal complex ratio (50 μM siSurv and 40 μM PA) was determined using electrophoresis (Fig. 2-13a). The loading capacity was 82%, as determined by UV-Vis spectroscopy (Fig. 2-13b). The siSurv-PA incorporated Lipos were attached to the MB (ML_{siSurv}) and then anchored and conjugated to MNP (Fe) and the HER2 antibody, as described previously.

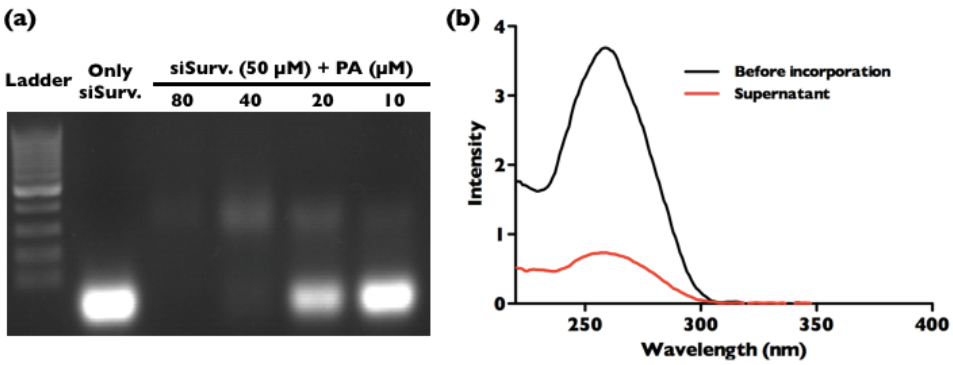

Figure 2-13. Electrophoresis results (a) for optimizing the conjugation reaction of PA and siSurv for gene delivery study and UV-vis spectrometer results (b) of siSurv content of original before loading reaction siSurv into liposome (black line) and supernatant after loading reaction (red line).

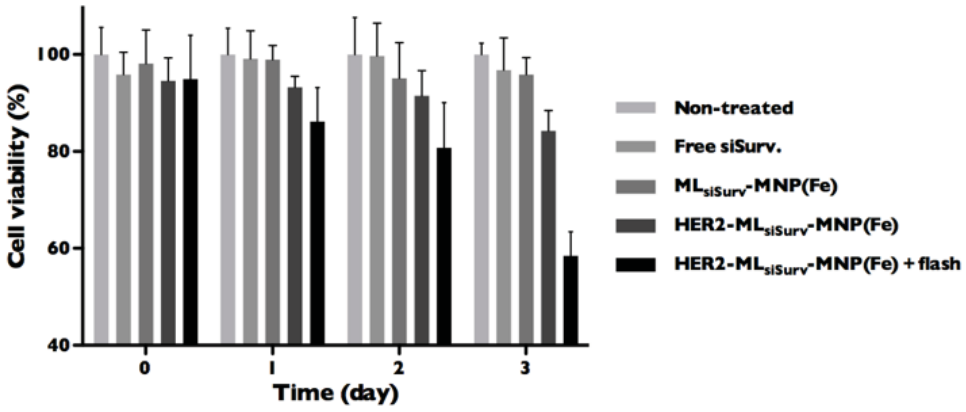

Figure 2-14. Cell viability of SkBr3 treated by complexes and US flash.

For therapeutic applications of siRNA delivery in vitro, the cell viability was monitored as a function of time and complexes. HER2-ML_{siSurv}-MNP (Fe) and US flash treated cells showed a significant decrease in viability (< 60 % viable) in 3 days, while the other controls showed maintained > 80 % viability (Fig. 2-14). The target gene showed 8-fold reduced expression levels, relative to the cells with siSurv only, as evident from PCR (Fig. 2-15). (All experiments were performed in triplicate.) These results showed that the MB-based particle system was able to enhance the selective transfection efficiency of the bio-molecules incorporated into the linked Lipo.

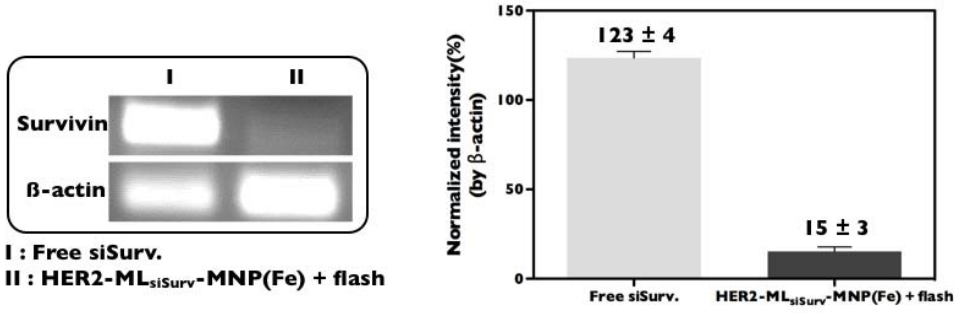

Figure 2-15. PCR results of SkBr3 treated by free siSurv and HER2-ML_{siSurv}-MNP (Fe) with US flash.

2.4. Conclusions

In summary, we have prepared a hybrid multifunctional complex comprising of MB, Lipo, and MNP (Fe). The resulting complexes showed high biocompatibility and selectivity, demonstrating multi-modal imaging capability for fluorescence, US, and MR. Interestingly, the linked therapeutic Lipos and MNPs (Fe) rapidly penetrated into the cancer cells after being exposed to US flash, and eventually enhanced the therapeutic effects and MR imaging due to MB cavitation and sonoporation. As a non-toxic theranostic material, the hybrid complex could be readily extended to US and MR-guided cancer treatment in clinical applications.[25]

2.5. References

1. Xie X., Lee S., Chen X., *Adv. Drug Delivery Rev.*, 62, 1064–1079 (2010).

2. Liu H. L., Fan C. H., Ting C. Y., Yeh C. K., *Theranostics*, 1, 432–444 (2014).

3. Prabhu P., Patravale V., *J. Biomed. Nanotechnol.*, 8, 859–882 (2012).

4. Wu W., Zhang Q., Wang J., Chen M., Li S., Lin Z., Li J., *Polym. Chem.*, 5, 5668–5679 (2014).

5. Wu W., Wang J., Lin Z., Li X., Li J., *Macromol. Rapid Commun.*, 35, 1679–1684 (2014).

6. Zhou Z., Wang L., Chi X., Bao J., Yang L., Zhao W., Chen Z., Wang X., Chen X., Gao J., *ACS Nano*, 7, 3287–3296 (2013).

7. Yoo H., Moon S. K., Hwang T., Kim Y. S., Kim J. H., Choi S. W., Kim J. H., *Langmuir*, 29, 5962–5967 (2013).

8. Gojova A., Guo B., Kota R. S., Rutledge J. C., Kennedy I. M., Barakat A. I., *Environ. Health Perspect.*, 115, 403–409 (2007).

9. Yang S. T., Liu J. H., Wang J., Yuan Y., Cao A., Wang H., Liu Y., Zhao Y., *J. Nanosci. Nanotechnol.*, 10, 8638–8645 (2010).

10. Yoke R., Grulke E., MacPhail R., *Wiley Interdiscip. Rev.: Nanomed. Nanobiotechnol.*, 5, 346–373 (2013).

11. Capece S., Chiessi E., Cavalli R., Giustetto P., Grishenkov D., Paradossi

G., *Chem. Commun.*, 49, 5763–5765 (2013).

12. Yang F. Y., Wong T. T., Teng M. C., Liu R. S., Lu M., Liang H. F., Wei M. C., *J. Controlled Release*, 160, 652–658 (2012).

13. Yoon Y. I., Kwon Y. S., Cho H. S., Heo S. H, Park K. S., Park S. G., Lee S. H., Hwang S. I., Kim Y. I., Jae H. J., Ahn G. J., Cho Y. S., Lee Hakho, Lee H. J., Yoon T. J., *Theranostics*, 4, 1133-1144 (2014).

14. Nguyen A. T., Wrenn S. P., *Wiley Interdiscip. Rev.: Nanomed. Nanobiotechnol.*, 6, 316–325 (2014).

15. Yang F., Li Y., Chen Z., Zhang Y., Wu J., Gu N., *Biomaterials*, 30, 3882–3890 (2009).

16. Ju K. Y., Lee J. W., Im G. H., Lee S., Pyo J., Park S. B., Lee J. H., Lee J. K., *Biomacromolecules*, 14, 3491–3497 (2013).

17. Prentice P., Cuschieri A., Dholakia K., Prausnitz M., Campbell P., *Nat. Phys.*, 1, 107–110 (2005).

18. Deng C. X., Sieling F., Pan H., Cui J., *Ultrasound Med. Biol.*, 30, 519–526 (2004).

19. Lee H., Dellatore S. M., Miller W. M., Messersmith P. B., *Science*, 318, 426–430 (2007).

20. Owen C., Patel N., Logie J., Pan G., Persson H., Moffat J., Sidhu S. S., Shoichet M. S., *J. Controlled Release*, 172, 395–404 (2013).

21. Manjappa A. S., Chaudhari K. R., Venkataraju M. P., Dantuluri P., Nanda

B., Sidda C., Sawant K. K., Murthy R. S., *J. Controlled Release*, 150, 2–22 (2011).

22 Hu Y., J. Wan M., Yu A. C., *Ultrasound Med. Biol.*, 39, 2393–2405 (2013).

23. Meijering B. D., Juffermans L. J., Wamel A., Henning R. H., Zuhorn I. S., Emmer M., Versteilen A. M., Paulus W. J., Gilst W. H., Kooiman K., Jong N., Musters R. J., Deelman L. E., Kamp O., *Circ. Res.*, 104, 679–687 (2009).

24. Arangoa M. A., Duzgunes N., *Gene Ther.*, 10, 5–14 (2003).

25. Yoon Y. I., Ju K. Y., Cho H. S., Yu K. N., Lee J. J., Ahn G. J., Lee S. H., Cho M. H., Lee H. J., Lee J. K., Yoon T. J., *Chem. Commun.*, 51, 9455-9458 (2015).

Chapter 3

Optimization of ultrasound parameters for microbubble-liposome complex-mediated delivery

3.1. Introduction

For the delivery of therapeutic materials into cells, various methods have been investigated, including electroporation, hydrodynamic delivery, ballistic delivery, and microinjection.[1] Delivery by ultrasound (US) has been evaluated to be an improved option.[2] US has many advantages, such as lack of invasiveness, safety, speed, and reduced cost. In addition, delivery by US has taken center stage in a new paradigm of image-guided therapy because the therapeutic contents can be loaded in microbubbles (MB).[3] A great deal of interest surrounds the use of US and MB for cancer therapy. In addition to high-resolution imaging, US shows powerful potential for image-guided therapy by MB-mediated delivery. The synergetic effect of US and MB used to carry US contrast agents makes sonoporation and delivery to cancer cells simple. Despite the many studies on US-mediated gene and drug delivery using MB[4], the conditions under which US-mediated delivery is most effective have not been determined.[5] Thus, the aim of this study is to optimize US treatment conditions to maximize the efficacy of delivery to cancer cells.

3.2. Experimental Section

3.2.1. Preparation of HER2-MB_G-$Lipo_R$ complex

To prepare HER2-MB-Lipo complex, the method introduced in chapter 1 was basically applied. To prepare MB including green fluorescent dye (G, fluorescein isothiocyanate, FITC, Sigma-Aldrich, St. Louis, MO, USA) and hydrophobic gas (SF_6 gas, Dong-A Industrial Gas, Seoul, Korea), DPPC (1,2-dihexadecanoyl-sn-glycero-3-phosphocholine, Avanti, Alabaster, AL, USA), DPPE (1,2-dipalmitorysn-glycero-3-phosphoethanolamine, Sigma-Aldrich), and DSPE-PEG-SPDP (1,2-distearoyl-sn-glycero-3-phosphoethanolamine-N-[PDP(polyethylene glycol)-2000], Avanti) were used.[6] H_2O was poured on film composed of DPPC, DPPE, DSPE-PEG-SPDP, and FITC and transferred to a hermetic vial (1.5-mL vial in vial file, Clr, PTFE Lnr, Wheaton, Millville, NJ, USA). After filling the vial with SF_6 gas, MB_G was prepared by using an amalgamator (JS 2001MX, KIMS, Incheon, Korea). $Liposome_R$ ($Lipo_R$) was produced using red fluorescent dye (R, Texas red, Sigma-Aldrich), DPPC, and DPPE. Texas red in H_2O was poured on the DPPC and DPPE film, and it was sonicated by a bath-type sonicator (4020P, Kodo Technical Research, Hwaseong, Korea). Unloaded Texas red was washed out by centrifugation (13,000 rpm, 5 minutes, twice). MB_G-$Lipo_R$ complex was prepared by

reacting $Lipo_R$ with MB_G for 2 hours. The unreacted components were washed out by centrifugation (13,000 rpm, 5 minutes, twice). After reaction of trastuzumab (Herceptin, Roche, Basel, Switzerland) with MB_G-$Lipo_R$ complex and centrifugation (13,000 rpm, 5 minutes, twice), HER2-MB_G-$Lipo_R$ complex was prepared.

3.2.2. Cancer cell culture

One of the most common breast cancer cell lines, SkBr3, was cultured using RPMI media (Life Technologies, Frederick, MD, USA), 10% fetal bovine serum (Life Technologies), and 1% penicillin streptomycin (37 °C, 5% CO_2; Life Technologies). In order to treat cells with HER2-MB_G-$Lipo_R$ complexes, the cells were seeded into a 1-well chamber slide (SPL, Pocheon, Korea).

3.2.3. US conditions

After delivering HER2-MB_G-$Lipo_R$ complexes to cells (1 h, 37 °C, 5 % CO_2), the complexes unattached to the cells were washed out by fresh media twice. For US treatment to the cells, a sonoporator (Sonidel, Dublin, Ireland) equipped with a 1-MHz probe was used. According to the intensity (w/cm^2),

time (min), and duty cycle (%) of the US machine, the cells were divided into eight groups: group A, 1 w/cm^2, 1 minute, 20%; group B, 1 w/cm^2, 1 minute, 60%; group C, 1 w/cm^2, 2 minutes, 20%; group D, 2 w/cm^2, 1 minute, 20%; group E, 1 w/cm^2, 2 minutes, 60%; group F, 2 w/cm^2, 1 minute, 60%; group G, 2 w/cm^2, 2 minutes, 20%; and group H, 2 w/cm^2, 2 minutes, and 60%. A control group, a group without antibody (Ab), and a group without US were also evaluated. The group without Ab was treated with MB_G-$Lipo_R$ complexes without Her2 Ab. The group without US was treated with HER2-MB_G-$Lipo_R$ complexes, but no US was applied.

Group	Intensity (W/cm^2)	Time (min)	Duty cycle (%)
A	**1**	**1**	**20**
B	**1**	**1**	**60**
C	**1**	**2**	**20**
D	**2**	**1**	**20**
E	**1**	**2**	**60**
F	**2**	**1**	**60**
G	**2**	**2**	**20**
H	**2**	**2**	**60**

Table 3-1. Groups classified by parameters of US machine.

3.2.4. Analysis of targeting and delivery effect

To confirm the targeting effect of Her2 antibody and delivery effect with various US parameters, a confocal laser scanning microscope (CLSM; Leica, Wetzlar, Germany) was used. To analyze FITC (excitation, 488 nm; emission, 500-570 nm) and Texas red (excitation, 594 nm; emission, 600-680 nm), 20× and 63× lenses were used. By using Leica Application Suite Advanced Fluorescence Lite, the software provided from the CLSM manufacturer, the fluorescence intensities inside and outside of the cell membrane were analyzed quantitatively. All experiments were performed in triplicate under equivalent conditions.

3.2.5. Statistical Analysis

One-way analysis of variance (ANOVA) was performed to evaluate the differences of fluorescence intensities in each group. All analyses were performed using IBM SPSS Statistics for Windows software, ver. 20 (IBM Co., Armonk, NY, USA).

3.3. Results

3.3.1. US phantom study of HER2-MB_G-$Lipo_R$ complex

HER2-MB_G-$Lipo_R$ complexes were successfully synthesized. Fig. 1 contains an image of a US echogenicity phantom study of HER2-MB_G-$Lipo_R$ complexes. Compared with distilled water (Fig. 3-1b), the US echogenicity image of HER2-MB_G-$Lipo_R$ complex (Fig. 3-1a) showed very high echogenicity.

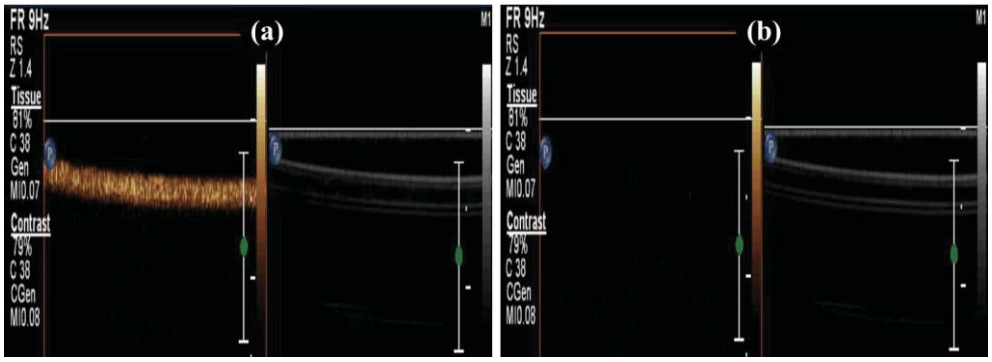

Figure 3-1. Phantom ultrasonogram of HER2-MB_G-$Lipo_R$ complex (a) and distilled water (b).

3.3.2. In vitro study for analysis of delivery by US conditions

Fig. 3-2 presented the set-up for the in vitro experiment using the US device. On a clean bench, the 1-MHz probe of the US generator was fixed by a support and clamp and placed on the cell dish containing cells.

Fig. 3-3 showed the CLSM results from the control group, the group without Ab, the group without US, and groups A-D. The control group contained only cells without any US insonication nor the addition of HER2-MB_G-$Lipo_R$ complex. The group without Ab contained cells treated by MB_G-$Lipo_R$ complex without Ab. The group without US contained cells treated by HER2-MB_G-$Lipo_R$ complex without US treatment. The control and group without Ab showed no fluorescent signal; on the other hand, the group without US showed fluorescent signals around the cells. The results of the above three groups indicated that HER2-MB_G-$Lipo_R$ complex was successfully synthesized and the targeting effect of the complex to the cells was strongly selective. The three parameters of US treatment were intensity (range, 1 to 2 w/cm^2), time (range, 1 to 2 minutes), and duty cycle (range, 20% to 60%). Group A was exposed to the lowest condition of each US parameter and group B was exposed to an intensified duty cycle only. Groups C and D underwent intensified time and intensity, respectively.

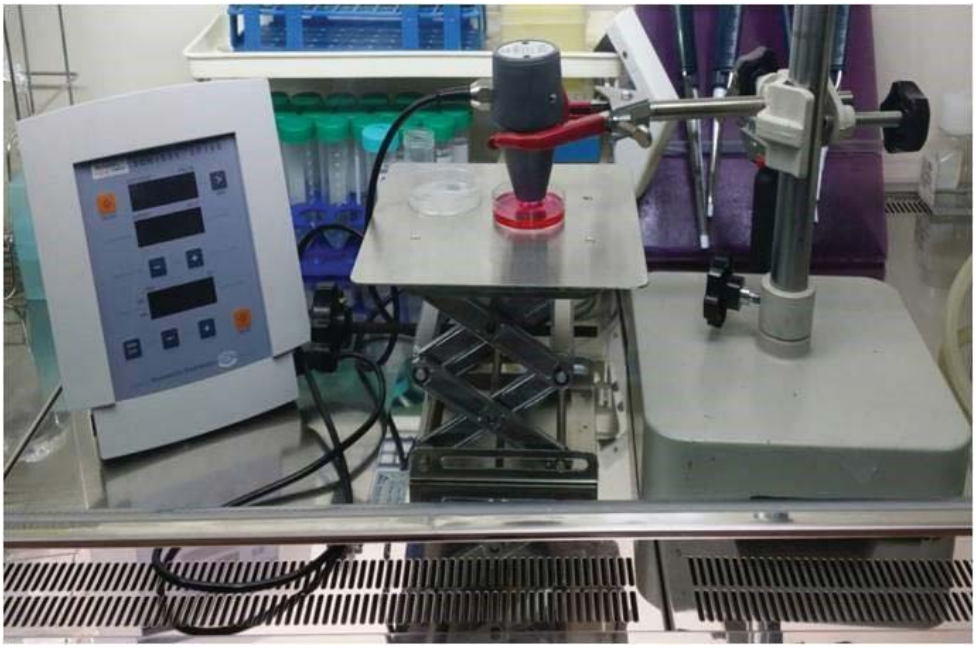

Figure 3-2. Set-up of ultrasound (US) experiments.

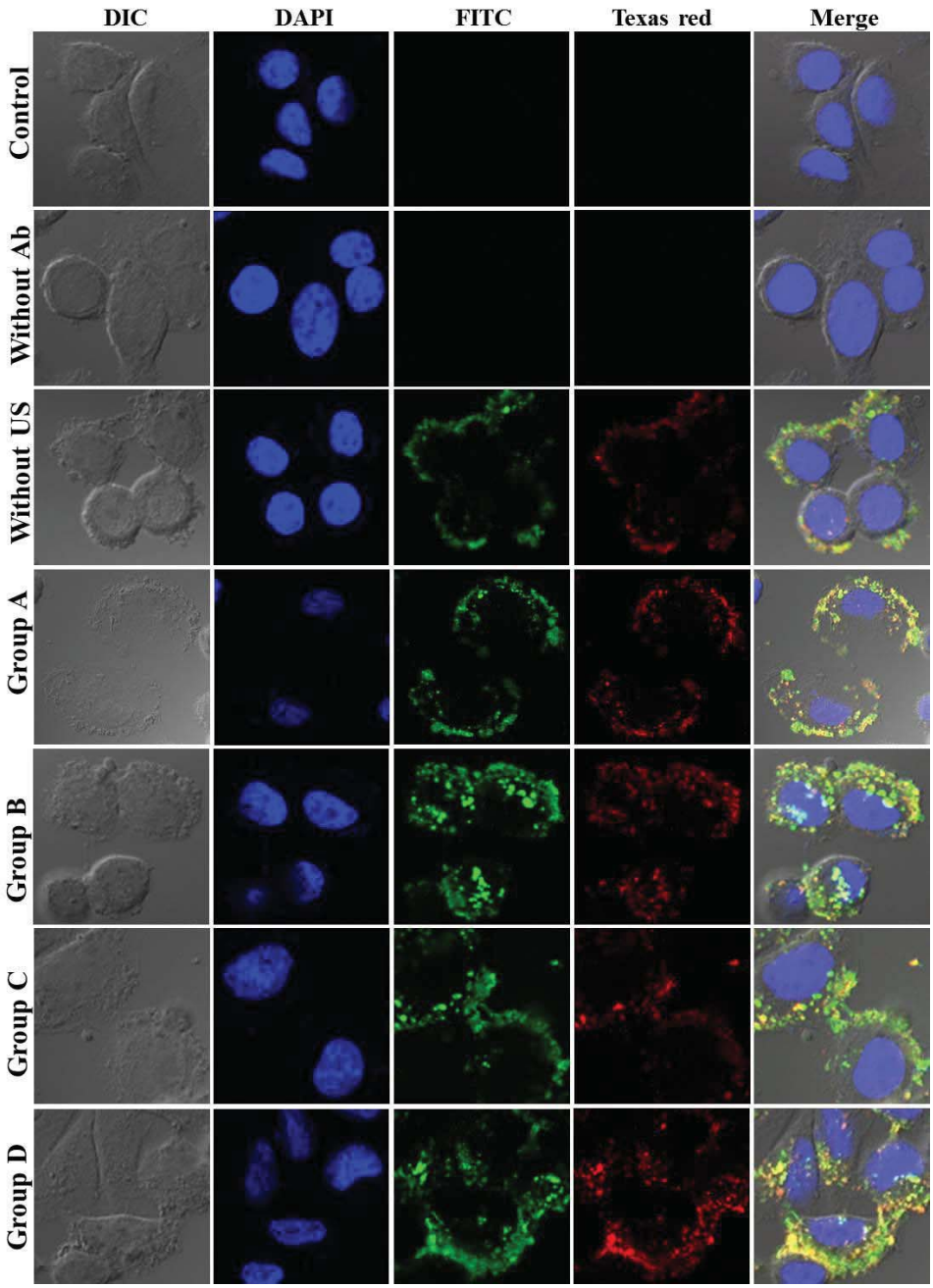

Figure 3-3. CLSM images of SkBr3 treated by HER2-MB_G-$Lipo_R$ complex in control, without Ab, without US, and groups (A-D).

Fig. 3-4 showed the CLSM results of the groups that were exposed to two or three intensified parameters at once. Fig. 3-5 showed the fluorescent intensity ratios. The basic US parameters were intensity, 1 w/cm^2; time, 1 minute; and duty cycle, 20%. With exposure to these basic US conditions, the proportion of the fluorescent intensity inside increased from 4.7% to 9.5% with FITC and from 5.6% to 14.5% with Texas red. By changing the duty cycle from 20% to 60%, the proportion of the fluorescent intensity on the inside increased from 9.5% to 91.0% with FITC and from 14.5% to 92.5% with Texas red. By changing the treatment time from 1 to 2 minutes, the proportion of the fluorescent intensity inside the cells increased from 9.5% to 50.5% with FITC and from 14.5% to 38.5 with Texas red. When I changed the intensity from 1 to 2 w/cm^2, the proportion of the fluorescent intensity inside increased from 9.5% to 86.0% with FITC and from 14.5% to 76.7% with Texas red. Among the three parameters, the parameter that was most important to optimize was the duty cycle since the fluorescent intensity ratio of group B was highest among groups A to D (Fig. 3-3). For delivery of FITC (i.e., the hydrophobic contents of MB), the groups with the most effective parameters were group E (1 w/cm^2, 2 minutes, 60 % duty cycle) and group H (2 w/cm^2, 2 minutes, 60%) (one-way ANOVA, $P < 0.001$, Tukey's honestly significant difference [HSD] was used as a post-hoc test). The fluorescent intensity ratios (inside the cells/outside the cells) were 95.9:4.1 in group E and

95.7:4.3 in group H (green, for FITC). Furthermore, for delivery of Texas red (i.e., the hydrophilic contents of the Lipo), the most effective parameters were those of group H (2 w/cm^2, 2 minutes, 60% duty cycle) (one-way ANOVA, $P < 0.001$, with Tukey's HSD used as a post-hoc test). The fluorescent intensity ratio was 95.0:5.0.

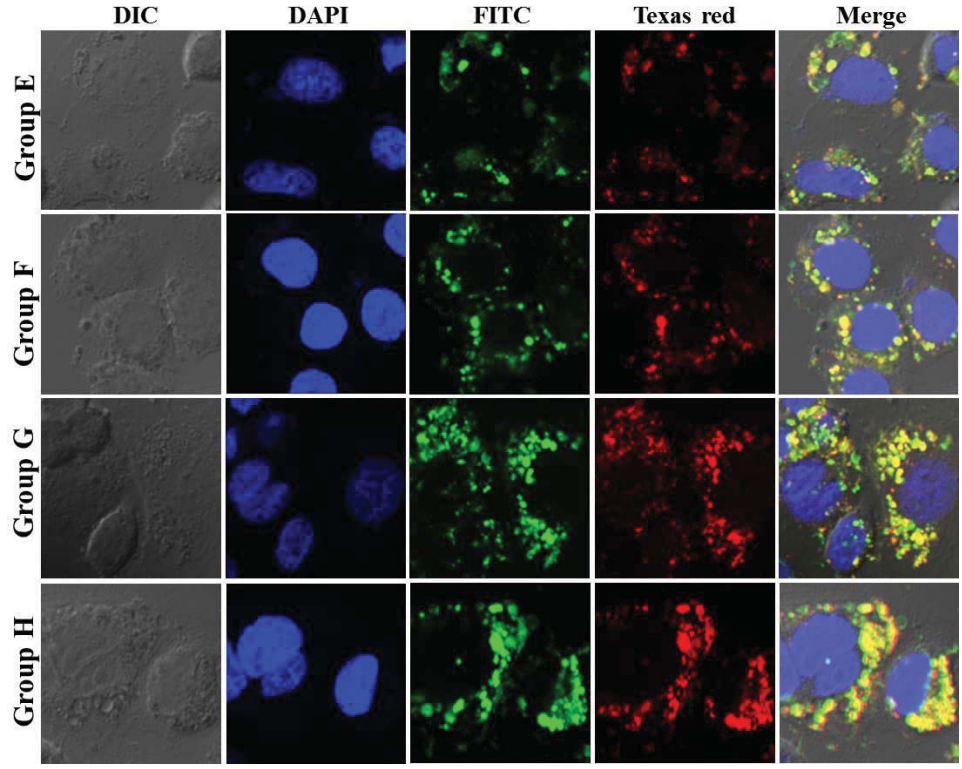

Figure 3-4. CLSM images of SkBr3 treated by HER2-MB_G-$Lipo_R$ complex in groups (E-H).

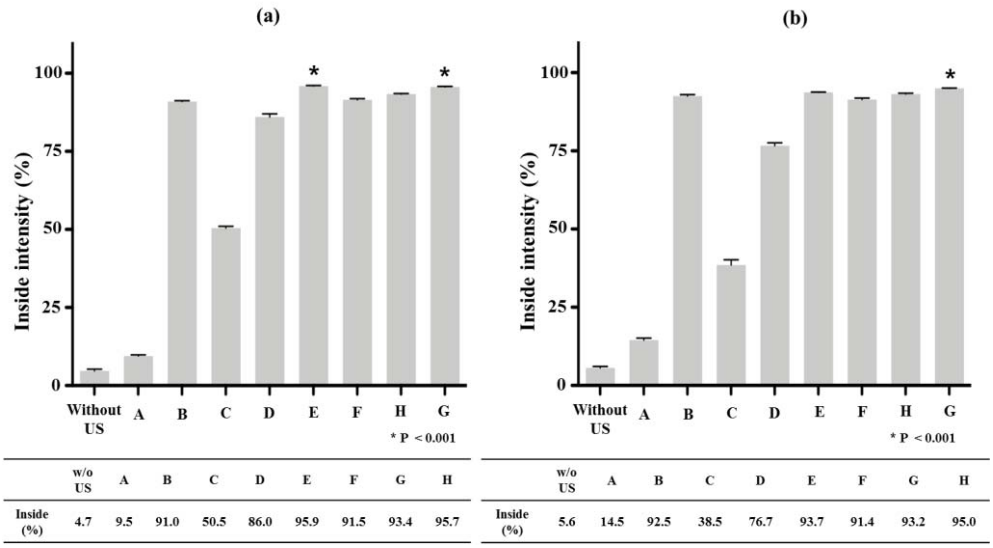

Figure 3-5. Graph showing the fluorescent intensity (%) of CLSM results by US parameters. (asterisk indicates the most effective conditions, one-way ANOVA, $P < 0.001$).

3.3. Discussion

MB, which are used as a contrast agent for US imaging in clinical diagnostics, comprise a gas-filled core and a shell of lipids or proteins. They range in size from 1 to 100 μm. Their gas component can generate echogenicity triggered by the US device because of the tendency of the layer to absorb or reflect US waves and nonlinear oscillation. The optimization of a variety of US conditions has a significant impact on the utilization of therapeutic US in many clinical settings.[7] Researchers have reported that sonoporation, the formation of temporary pores in the cell membrane, enhanced endocytosis. Qin et al.[8] reported that sonoporation achieved disruption of the plasma membrane for delivery of fluorescent dye in HeLa cancer cells. Delalande et al.[9] and Fan et al.[10] noted that the use of US and MB for sonoporation is being considered an emerging method for achieving localized drug and gene delivery. Owing to the variety of US conditions used and corresponding MB behavior, optimization of US conditions is essential.[11-13] When MB are transiently exposed to the proper US intensity, time, and duty cycle, the MB contract or collapse, simplifying delivery. Fan et al.[14] reported US parameters in experiments including acoustic pressures of 0.06-0.6 MPa, pulse repetition frequency of 10 Hz-1 KHz, and duty cycles of 0.016 % - 20 %. The total duration of US application was 1 second. Comparison of the

delivery outcomes indicated that high acoustic pressure was the most powerful parameter for intracellular delivery. For Yan et al.[15], the parameters were times from 5 seconds to 60 seconds and acoustic pressures from 0.35 to 1.0 MPa. The duty cycle of US application was 50%. The above results were meaningful, but they provided no precise protocol for the most effective delivery in vitro. In this study, we focused on setting US conditions for the most efficient delivery to cells. I used a US generator, a sonoporator (SP100, Sonidel), equipped with a 1-MHz probe. The radius of the probe (bottom) was 75 mm. This US generator had variable controls for time, intensity, and duty cycle. A duty cycle is defined as the percentage of one period in which a signal is active. For example, if an electrical device runs for 50 out of 100 seconds, its duty cycle is 50%. For this study, HER2-MB_G-$Lipo_R$ complex including FITC in MB and Texas red in Lipo and binding Ab was synthesized. Because FITC is hydrophobic, it should be contained in MBs, whereas Texas red is hydrophilic, so it should be contained in Lipos. As can be seen in Fig. 3-1a, HER2-MB_G-$Lipo_R$ complex showed high echogenicity, showing the possibilities as a US contrast agent, and furthermore, as a vehicle for gene and drug delivery. As shown in Fig. 3-3, the high targeting effect of HER2-MB_G-$Lipo_R$ complex to cells was verified. When cells were treated with MB_G-$Lipo_R$ complex without Ab, no fluorescence appeared (“without Ab group” of Fig. 3-3). In contrast, when cells were treated with HER2-MB_G-$Lipo_R$ complex,

intense green (FITC) and red (Texas red) fluorescence appeared around the cell membrane ("without US group" of Fig. 3-3). It showed that MB-mediated delivery can be more effective with an active targeting strategy. Tanizaki et al.[16] and Weigelt et al.[17] reported on the targeting effect of Her2 Ab to SkBr3. Depending on various US conditions, the delivery effect to the inside of the cell membrane after US was confirmed. The US parameters were intensity (w/cm^2), time (minutes), and duty cycle (%). This study found that the most powerful US parameter was duty cycle, followed by intensity, and then time (Fig. 3-5). A synergetic effect among parameters also existed. Group E (1 w/cm^2, 2 minutes, and 60 % duty cycle) (Fig. 3-4) showed the most powerful effect of FITC delivery to the cells. FITC in MB can substitute for many other hydrophobic therapeutic materials. To deliver hydrophobic therapeutic materials, for example, paclitaxel for cancer therapy, the condition of 1 w/cm^2, 2 minutes, and 60 % duty cycle was found to be most suitable in our experiments. Group H (2 w/cm^2, 2 minutes, and 60% duty cycle) (Fig. 3-4) showed the most powerful effect for FITC and Texas red co-delivery to cells. Texas red, which was carried by Lipos, can be used as a substitute for many hydrophilic therapeutic materials such as doxorubicin or genetic therapeutic materials. To deliver hydrophobic and hydrophilic therapeutic materials for therapy, the condition of 2 w/cm^2, 2 minutes, and 60% duty cycle were the best among tested conditions. This study has several limitations. First,

experiments were limited to in vitro studies. Therefore, future experiments should investigate optimal parameters for in vivo conditions. Second, parameters depended on the US machine, so I had only a few options for settings; for more exact information regarding optimal conditions, this study need to measure the acoustic pressure at each setting.

3.4. Conclusions

This study confirmed that HER2-MB_G-$Lipo_R$ complex was successfully synthesized. An active targeting method, such as attaching Her2 Ab, was useful in MB-mediated delivery. Results with varying US parameters in vitro verified that the duty cycle played the most powerful role in delivery into cancer cells in these experiments. These results should provide a basis for establishing reference parameters for performing gene and drug delivery studies using MB and US under in vitro conditions. Future improvements in US techniques combined with new developments of contrast agents containing therapeutic materials such as drugs and genes will make US a more powerful therapy modality in addition to its role as an imaging modality.[18]

3.5. References

1. Wells D. J., *Gene Ther.*, 11, 1363-1369 (2004).

2. Newman C. M., Lawrie A., Brisken A. F., Cumberland D. C., *Echocardiography*, 18, 339-347 (2001).

3. Blomley M. J., Cooke J. C., Unger E. C., Monaghan M. J., Cosgrove D. O., *B. M. J.*, 322, 1222-1225 (2001).

4. Lawrie A., Brisken A. F., Francis S. E., Tayler D. I., Chamberlain J., Crossman D. C., *Circulation*, 99, 2617-2620 (1999).

5. Miller D. L., Quddus J., *Ultrasound Med. Biol.*, 26, 661-667 (2000).

6. Yoon Y. I., Kwon Y. S., Cho H. S., Heo S. H, Park K. S., Park S. G., Lee S. H., Hwang S. I., Kim Y. I., Jae H. J., Ahn G. J., Cho Y. S., Lee Hakho, Lee H. J., Yoon T. J., *Theranostics*, 4, 1133-1144 (2014).

7. Liu J. B., Wansaicheong G., Merton D. A., Forsberg F., Goldberg B. B., *J. Med. Ultrasound*, 13, 109-126 (2005).

8. Qin P., Xu L., Hu Y., Zhong W., Cai P., Du L., *Ultrasound Med. Biol.*, 40, 979-989 (2014).

9. Delalande A., Kotopoulis S., Postema M., Midoux P., Pichon C., *Gene*, 525, 191-199 (2013).

10. Fan Z., Kumon R. E., Park J., Deng C. X., *J. Control. Release*, 142, 31-39 (2010).

11. Hensel K., Siepmann M., Haendschke K., Emmelmann S., Daigeler A., Hauser J., *IFMBE Proc.*, 22, 1422-1425 (2009).

12. Lentacker I., De Cock I., Deckers R., De Smedt S. C., Moonen C. T., *Adv. Drug Deliv. Rev.*, 72, 49-64 (2014).

13. Lin C. R., Chen K. H., Yang C. H., Cheng J. T., Sheen-Chen S. M., Wu C. H., *J. Biomed. Sci.*, 17, 44 (2010).

14. Fan Z., Chen D., Deng C. X., *Ultrasound Med. Biol.*, 40, 1260- 1272 (2014).

15. Yan F., Li L., Deng Z., Jin Q., Chen J., Yang W., *J. Control. Release*, 166, 246-255 (2013).

16. Tanizaki J., Okamoto I., Takezawa K., Tsukioka S., Uchida J., Kiniwa M., *Mol. Cancer Ther.*, 9, 1198-1207(2010).

17. Weigelt B., Lo A. T., Park C. C., Gray J. W., Bissell M. J., *Breast Cancer Res. Treat.*, 122, 35-43 (2010).

18. Yoon Y. I., Yoon T. J., Lee H. J., *Ultrasonography*, 34, 297-303 (2015).

Korean Abstract

생물학적 응용이 가능한 진단·치료용 입자 시스템에 관한 연구

윤 영 일

융합과학부 나노융합전공

서울대학교 대학원

임상적으로 사용되는 초음파 영상 (Ultrasound imaging) 진단은 인간의 귀에 들리지 않는 높은 주파수의 음파를 인체 표면에서 인체 내부로 보낸 후, 반사되어 돌아오는 음파를 검출기로 영상화 하여 이루어진다. 이러한 초음파 검사는 다른 영상기기에 (예: 자기공명장치, 컴퓨터 단층촬영장치, 양전자 방출단층촬영장치) 비해

인체에 무해하며, 통증을 유발하지 않고 신속하게 실시된다. 하지만, 다른 영상기기에 비해 낮은 분해능을 보완하기 위해서 초음파 조영제가 사용된다. 현재 임상에서 사용되는 초음파 조영제는 단순한 진단을 목적으로 하고 있지만, 이번 연구는 진단과 치료를 동시에 실시하는 진단·치료 (Theranostic) 분야를 타켓함으로서 초음파를 매개로 하는 새로운 치료법의 패러다임을 제시하고자 하였다. 또한, 초음파 조영제와 특정 세기의 초음파에 의해 일시적으로 발생되는 초음파천공법을 (Sonoporation) 접목하여 보다 효과적인 치료법을 소개하였다.

HER2 양성 유방암세포를 선택적으로 인지하고 항암제 및 유전자 치료제를 함유하는 복합체를 제조하였으며, 제조된 복합체를 특성분석 할 수 있는 다양한 분석장비를 이용하여 확인하였다. 암세포를 대상으로 하는 세포내 연구 그리고 종양토끼 동물모델을 대상으로 하는 생체내 연구 수준에서 우수한 진단 및 치료 효과를 확인하였다.

진단시 분해능의 한계를 보완하기 위해서, 위의 초음파 진단 및 치료용 복합체에 자기공명영상 진단 기능이 있는 철 이온을 함유하는 멜라닌 나노입자가 결합된 새로운 복합체를 제조하였다. 이로써, 진단의 영역에서 초음파와 자기공명영상 장치를 동시에

이용하여 서로의 장점을 부각시키고, 단점을 보완하여 보다 정확하고 신속한 진단이 가능한 분야를 소개하였다. 또한, 복합체에 유전자 치료제를 포함시킴으로써 듀얼 진단 및 치료제를 제조하였고, 세포내 연구를 통해서 그 우수한 효과를 확인하였다.

약물전달을 위해서, 휴대용 초음파 발생장치의 인자들을 (강도 (w/cm^2), 시간 (minute), 듀티 사이클 (%)) 최적화하는 것은 소수성 및 친수성 치료제를 효과적으로 암세포에 전달 할 수 있는 가능성을 보여주는 것으로 확인되었다.

종합적으로 이번 연구에서는 생물학적 응용이 가능한 진단•치료용 입자 시스템에 관한 연구가 진행되었다. 팬텀, 세포내 그리고 생체내 연구를 통해서, 암에 대한 우수한 초음파 그리고 자기공명영상 진단 효과 및 치료 효과를 확인하였다.

주요 핵심어: 마이크로 버블, 리포좀, 멜라닌 나노입자, 초음파 조영제, 자기공명영상 조영제

학번: 2011-30755